DEPARTMENT OF PHYSICS
UNIVERSITY OF JYVÄSKYLÄ
RESEARCH REPORT No. 6/2005

DENSITY-FUNCTIONAL STUDIES OF COUPLED QUANTUM DOT STRUCTURES

BY
KIMMO KÄRKKÄINEN

Academic Dissertation
for the Degree of
Doctor of Philosophy

To be presented, by permission of the
Faculty of Mathematics and Natural Sciences
of the University of Jyväskylä,
for public examination in Auditorium FYS-1 of the
University of Jyväskylä on August 12, 2005
at 12 o'clock noon

Jyväskylä, Finland
June 2005

ISBN 978-951-39-3163-6
URN:ISBN:978-951-39-3163-6

Preface

This work has been carried out at the Department of Physics and the Nanoscience Center in the University of Jyväskylä during the years 2002-2005.

I would like to start by thanking my supervisor Professor Matti Manninen for his competent and motivating guidance throughout the work, Doctor Matti Koskinen for inspiring and educative discussions about numerical methods in density-functional theory and Doctor Stephanie Reimann for fruitful collaboration and hospitality during my visit at the University of Lund.

It has been a priviledge to work with Kirsi Manninen, Kari Rytkönen and Pekka Koskinen. Their support has been invaluable. Warmest thanks go to the whole staff at the department for providing a pleasant and open atmosphere and for help with practical issues.

Financial support provided by the Finnish Science Academy is also greatly acknowledged.

I want to thank my parents for their love and support. Finally, I thank my beloved wife Anne for walking the uphills and downhills alongside me and our daughter Eeva for bringing sunshine to rainy days.

Jyväskylä, June 2005

Kimmo Kärkkäinen

Abstract

Semiconductor quantum dots have established their position as testing laboratories for many-body quantum effects. Artificial tuning of external parameters makes the physics of quantum dots particularly interesting. The number of confined electrons or the strength of the confining potential can be varied and, consequently, the characteristics of the quantum mechanical state can be changed.

In this Thesis, we employ the density-functional theory to examine the electronic and magnetic properties of coupled quantum dot structures. We develop an exchange-correlation energy functional to be used in the density-functional calculations of coupled systems. We study vertical electron-hole quantum dot molecules, one-dimensional quantum dot arrays and multicomponent quantum dots in which the carriers could belong to the different bands of the semiconductor material.

Computational studies of complex coupled quantum dot structures call for efficient numerical methods. To be used as the computational tool, we chose the Kohn-Sham formulation of the density-functional theory in which the exchange and correlation effects are treated within local approximation. We believe that the density-functional theory gives a satisfactory qualitative picture of the many-body effects governing the physics of coupled quantum dots.

List of Publications

I K. Kärkkäinen, M. Koskinen, M. Manninen, and S.M. Reimann, *Electron-hole bilayer quantum dots: phase diagram and exciton localization*, Solid State Comm. **130** (2004) 187-191

II K. Kärkkäinen, M. Koskinen, S.M. Reimann, and M. Manninen, *Exchange-correlation energy of a multicomponent two-dimensional electron gas*, Phys. Rev. B **68**, 205322 (2003)

III K. Kärkkäinen, M. Koskinen, S.M. Reimann, and M. Manninen, *Density-functional theory of multicomponent quantum dots*, Phys. Rev. B **70**, 195310 (2004)

IV K. Kärkkäinen, M. Koskinen, S.M. Reimann, and M. Manninen, *Magnetism in one-dimensional quantum dot arrays*, cond-mat/0505036

The author has written the drafts of all the manuscripts, has performed the numerical work of publications I,II and IV and assisted with the numerical work of publication III. The author has also participated in computer code development needed for publications III and IV.

Contents

1 Semiconductor Quantum Dots

1.1 Introduction

Since their discovery in the 1970s the low-dimensional semiconductor nanostructures have evolved from scientific curiosities to means of probing the quantum mechanical many-body effects and to modern devices with an exciting application potential. The many-body quantum effects are regularly studied in heterostructured nanodevices that act as electron traps or wave-guides. Experiments as well as theoretical studies have revealed the microscopic nature of these devices and active research brings along also commercially interesting innovations.

Despite the giant leaps in the progress of fabrication and measuring techniques in the nanometer-sized devices the inter-particle correlations make the physics and the experiments challenging. Numerical modelling can give some insight into the many-body effects observed in experiments. However, due to the complexity of nanostructures, modelling requires well-justified simplifications in order to make the problem tractable. Often the problem is reduced to finding the eigenspectrum of the many-body Hamiltonian, which can only be done numerically for a relatively small number of particles. Paul Dirac, one of the pioneers in the many-body quantum mechanics, has commented on the difficulty of this task:

> "The underlying physical laws necessary for the mathematical theory of a large part of physics and the whole of chemistry are thus completely known, and the difficulty is only that the exact application of these laws leads to equations much too complicated to be soluble."

Since Dirac's days methods and computers have evolved to a level where problems of several electrons can be solved. One milestone in this development has been the Kohn-Sham formulation of the density-functional theory, which can be used in ground-state calculations of systems containing up to hundreds of electrons.

Quantum dots are ideal candidates for probing many-body effects theoretically and experimentally. With modern fabrication methods one can confine a tunable number of electrons into a small island. The size of the island can be made comparable to the de Broglie wavelength of an electron so that a true quantum confinement can be

achieved. Consequently, quantum dots have a microscopic shell structure that can be revealed in transport measurements. Due to this similarity to real atoms, quantum dots are often called artificial atoms.

Trend in the studies of quantum dot structures has been to prepare evermore complex devices using, for example, self-assembly [3, 9]. Coupled quantum dots are interesting also in studies of quantum computing in which two-state systems are needed for realisation of qubit [10, 11]. Investigation of these structures with numerical methods involves solving rather large problems accurately and yet in a reasonable time-span. The density functional theory has proven its quality in studies of large atomic clusters and has also constantly been used in quantum dot modelling.

In this thesis, we employ the Kohn-Sham method to view the many-body ground-state effects in different quantum dot structures. In this chapter, we review the fabrication and experimental methods of quantum dots and discuss the approximations needed for quantum dot models. In Chapter 2, we present the basics of the Kohn-Sham formulation of the density-functional theory, discuss numerical methods and review briefly other methods used in electron structure calculations. Chapters 3-5 deal with the results presented in publications [I]-[IV].

1.2 Fabrication and Experiments

Two-Dimensional Electron Gas

Two-dimensional electron gas can be formed in the heterojunction between two dissimilar semiconductor alloys [12]. A prototypical heterojunction can be prepared by depositing a thin layer of AlGaAs alloy on a GaAs layer with molecular beam epitaxy technique, which allows an atomic scale precision in layer composition. There are no appreciable lattice distortions on the junction since the lattice constants and structures of GaAs and AlAs are identical, but the band gaps of AlGaAs and GaAs alloys are different. Charge transfer across the junction interface will adjust the chemical potential constant throughout the junction. Consequently, the band edges bend giving rise to a potential barrier on the GaAs side. By sufficient doping, the chemical potential reaches this potential well, and the conduction electrons will be trapped on the vicinity of the interface. The motion of the electrons parallel to the interface will remain free and the resulting electron gas is dynamically two-dimensional if only the lowest perpendicular state is occupied. Due to the shallowness of the confinement well, the experiments on two-dimensional electron gas are usually performed at temperatures of few kelvins down to millikelvins.

Lateral Quantum Dots in Heterostructures

The motion of electrons in two-dimensional electron gas can be restricted further by etching and gate patterning techniques. Lithographic patterning of metallic gates or electrodes on top of the heterostructure can be used to define lateral quantum dots containing several hundred electrons. The electrons in the two-dimensional electron gas are repelled by the negative voltage applied to the gate electrodes and, with suitable geometry, the electrons can be clenched into a small island [13]. The number of confined electrons can be tuned by changing the gate voltage. Earlier the lower bound for the number of confined electrons was limited to few tens of electrons, but the modern techniques in gate patterning allow also few-electron confinement. Recently, Elzerman *et al.* have reported a realization of a gate patterned few-electron double quantum dot in AlGaAs/GaAs heterostructure [10].

Microscopic Shell Structure of Vertical Quantum Dots

Etching techniques are well-suited for fabricating pillar shaped few-electron quantum dots. In the very first devices, electron beam lithography was used for defining pillars in AlGaAs/GaAs heterostructure. By attaching electric contacts at the ends of the pillar, Reed *et al.* were able to measure electron transport oscillations in a vertical quantum dot caused by Coulomb blockade effect [14]. Tarucha *et al.* were the first to reveal the microscopic shell structure of vertical quantum dots in electron transport measurement [15]. The quantum dot setup they used is shown in Figure 1.1. A double-barrier heterostructured pillar is surrounded by a metallic voltage-biased Schottky gate, which allows a full control over the lateral confinement and enables single-electron charging of the dot. By measuring current through the pillar as a function of gate voltage V_g Tarucha *et al.* observed Coulomb oscillations resulting from one by one addition of electrons to the dot. The conductance peaks were not equidistant but their spacing depended on the electron number N. The voltage spacing between the current peaks is proportional to the addition energy, which measures the changes of electrochemical potential as a function of the electron number. Addition energy spectrum shows pronounced maxima at $N = 2, 6$ and 12. These "magic" electron numbers are related to the microscopic shell structure of the quantum dot.

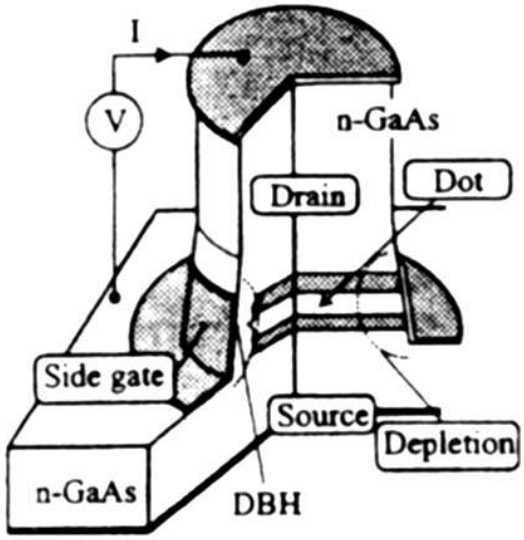

Figure 1.1: Schematic view of a vertical quantum dot. The dot is located between two heterostructure barriers and is surrounded by a Schottky gate. The number of confined electrons can be tuned by varying gate voltage V_g.

1.3 Modelling Vertical Quantum Dots

Successful modelling of a quantum dot involves few well-justified approximations to make the model tractable. The simplifications lead to the fundamental problem of condensed matter physics, that is, the problem of solving the many-body Schrödinger equation.

Approximations

The pillar shaped vertical quantum dot described in the previous section has a diameter ten times longer than its thickness, and the experiments are performed at around 50 mK. Therefore, one can assume that the confined electrons occupy only the lowest state in the z-direction (along the pillar) and the dot is a smoothly confined circular electron island in two-dimensional plane. The "magic" electron numbers coincide with the closed shells of the circular two-dimensional harmonic oscillator giving a hint that the confinement is parabolic to a good approximation.

The confined electrons originate from the conduction band of the semiconductor, and only the bottom of the band is populated by the conduction electrons. In the *effective mass approximation*, the minimum is approximated with a parabolic dispersion

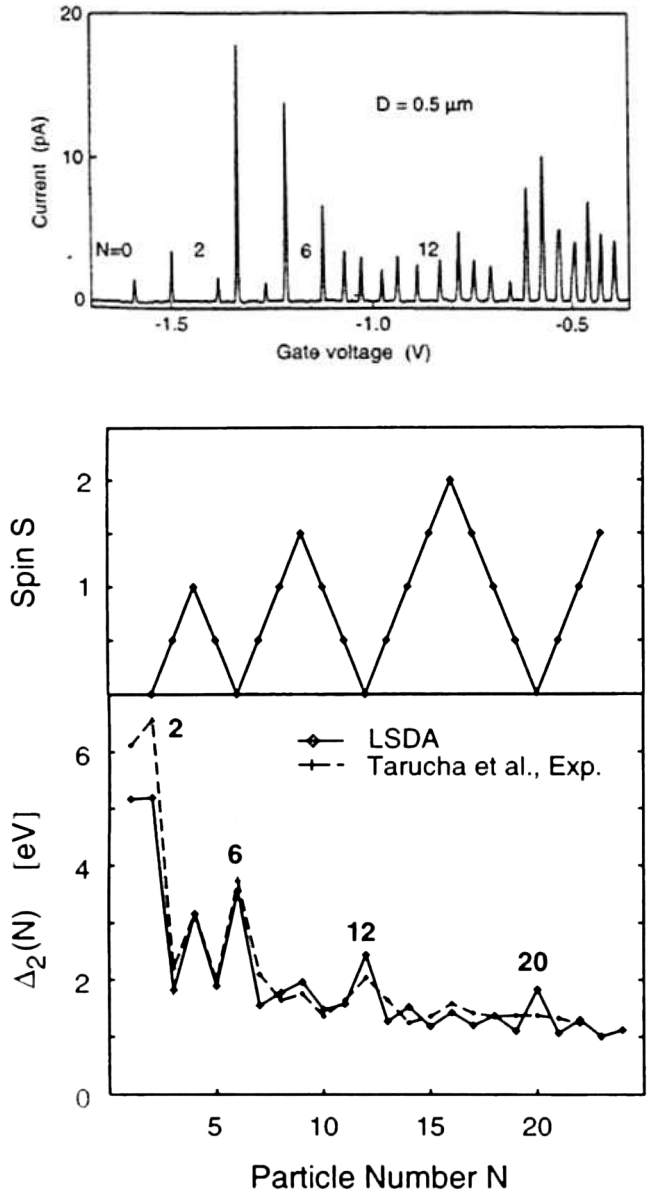

Figure 1.2: Upper: Coulomb oscillations in the linear transport through a vertical quantum dot. Peak separation depends on the electron number N, and it is especially long for $N = 2, 6$, and 12. Lower: Addition spectrum of a vertical quantum dot. The addition energy spectrum computed from the spin density-functional theory (solid line) compares well to the measured spectrum (dashed line) [16].

relation with curvature determined by the effective mass m^*. The screening of the Coulomb interaction by the ions of the lattice is taken into account in the dielectric constant ϵ.

Hamiltonian for a Quantum Dot

In the approximations described above, parameters m^* and ϵ include the complicated bandstructure effects of the underlying lattice. In the resulting model, the quantum dot is treated as a two-dimensional electron system confined into external potential $v_{ext}(\boldsymbol{r})$, where $\boldsymbol{r} = (x, y)$. In the absence of an external magnetic field, the Hamiltonian for the quantum dot with N electrons reads

$$H = \sum_{i=1}^{N} \left(\frac{\boldsymbol{p}_i^2}{2m^*} + v_{ext}(\boldsymbol{r}_i) \right) + \frac{1}{2} \sum_{i \neq j} \frac{e^2}{4\pi\epsilon_0 \epsilon |\boldsymbol{r}_i - \boldsymbol{r}_j|}. \tag{1.1}$$

The first of the two terms consists of the kinetic energy and the external harmonic confinement,

$$v_{ext}(\boldsymbol{r}) = \frac{1}{2} m^* \omega^2 r^2, \tag{1.2}$$

while the second two-body term incorporates Coulomb interaction between the electrons. The Hamiltonian is often written in terms of effective atomic units, where $\hbar = 4\pi\epsilon\epsilon_0 = m^* = e = 1$. Then, the units of energy and length are effective Hartree $\mathrm{Ha}^* = m^* e^4 / \hbar^2 (4\pi\epsilon\epsilon_0)^2$ and effective Bohr radius $\mathrm{a}_0^* = \hbar^2 (4\pi\epsilon\epsilon_0)/m^* e^2$, respectively.

The complications in solving the many-body problem arise from the correlations caused by the electrostatic repulsion between the particles and the antisymmetry requirement of the wave function. There are several methods available for attacking the correlated few-electron problem. We will discuss those in the following chapter.

The analytically soluble single-particle part of the Hamiltonian (1.1) is the starting point of quantum dot modelling and it also yields some qualitative features of the interacting system. The single-particle wave functions in the two-dimensional harmonic potential are

$$\phi_{nm}(r, \theta) = \sqrt{\frac{n!}{(n + |m|)!}} \frac{1}{\sqrt{\pi} l_0} \left(\frac{r}{l_0} \right)^{|m|} \exp(-r^2/2l_0^2) L_n^{|m|}(r^2/l_0^2) e^{im\theta}. \tag{1.3}$$

Here $L_n^{|m|}$ is a Laguerre polynomial and $l_0 = \sqrt{\hbar/m^*\omega}$ is the oscillator length. In the presence of magnetic field perpendicular to the plane, the oscillator length is replaced by $l_B = \sqrt{\hbar/m^*\Omega}$, where $\Omega^2 = \omega^2 + \omega_c^2/4$ and $\omega_c = eB/m^*$ is the cyclotron frequency.

Due to the circular symmetry of the potential, the orbital angular momentum m is a good quantum number. As the motion is restricted to two dimensional plane, the angular momentum will concur with its z-component, thus $m = 0, \pm 1, \pm 2, \ldots$ The principal quantum number n tells the number of nodes of the radial part of the wave function and, therefore, takes values $n = 0, 1, 2, \ldots$ The corresponding single-particle energies are

$$\varepsilon_{nm} = \hbar\omega(2n + |m| + 1). \tag{1.4}$$

The single-particle spectrum is visualised in Figure 1.3, in which we see that the degeneracy of the lth shell is $2l$, where $l = 1, 2, \ldots$, and factor 2 stems from spin. If we occupy the 2D oscillator levels with non-interacting electrons, we notice that shell closures occur at electron numbers $N = 2, 6, 12, \ldots$, and they coincide with the "magic numbers" in the addition energy spectrum of Figure 1.2. The main effect of the Coulomb interaction is to maximise spin due to Hund's first rule at open shell electron numbers $N = 4, 9, 16 \ldots$ These numbers correspond to the maxima in the addition spectrum.

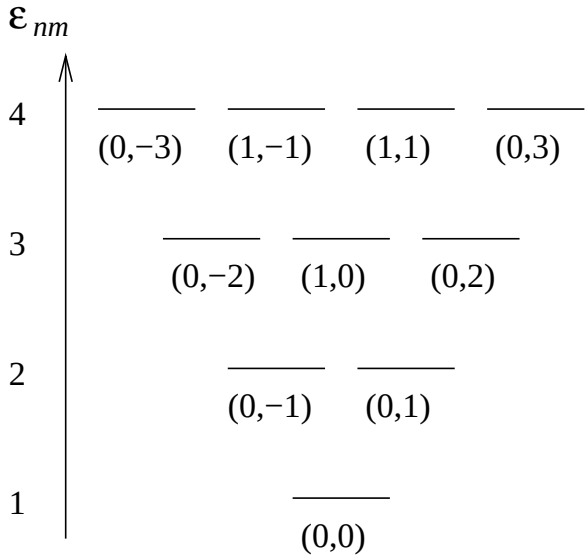

Figure 1.3: Lowest s, p, sd and fp shells of the two-dimensional harmonic potential. The quantum numbers for each state are shown in parentheses (n, m)

2 Density-functional Theory in Quantum Dot Modelling

Density-functional theory (DFT) in its self-consistent formulation by Kohn and Sham is one of the most frequently used methods in quantum dot modelling and in electronic structure studies of condensed matter in general. The strength of the theory resides in the observation of Hohenberg and Kohn that the electron density can be used to determine the ground state instead of the many-electron wave function. The quantum mechanical N-electron wave function needs N spatial and spin variables for its complete description while the density is a real valued function of a single spatial variable. This huge reduction in the degrees of freedom makes the many-body problem soluble at least in principle. In practice the accuracy of the method is dependent on the approximations needed to take into account the exchange and correlation effects that become all-important in the description of few-electron low-density quantum dots.

2.1 Principles

The Hohenberg-Kohn Theorem

The many-body Hamiltonian (1.1) incorporates operators for the kinetic energy, the external potential and the pair interaction between the electrons, that is,

$$H = T + V_{ext} + U_{ee}. \tag{2.1}$$

The energy of the electron system in state Ψ is given by the expectation value of the Hamiltonian, $E[\Psi] = \langle\Psi|H|\Psi\rangle$, when the wave function is normalised, that is, $\langle\Psi|\Psi\rangle = 1$. According to the variational principle, the ground state Ψ_0 yields the lowest energy. Thus, the variational minimisation of $E[\Psi]$ with respect to all the allowed N-electron wave functions will yield the exact ground state Ψ_0.

Instead of searching the whole Hilbert space of wave functions in order to find the ground state, we may as well search for the ground state density [8]. This is justified by the Hohenberg-Kohn theorem stating that the energy of the interacting electrons can be written as a functional of the electron density n, and that the minimisation of the resulting functional with respect to the density yields the nondegenerate ground

state density which has a one-to-one correspondence to the external potential v_{ext} [17]. The densities qualifying this Hohenberg-Kohn criterion are called v-representable and the functional to be minimised is

$$E[n] = \langle \Psi[n] | T + V_{ext} + U_{ee} | \Psi[n] \rangle = F[n] + \int n(\boldsymbol{r}) v_{ext}(\boldsymbol{r}) \mathrm{d}\boldsymbol{r}, \tag{2.2}$$

where $F[n] = \langle \Psi[n] | T + U_{ee} | \Psi[n] \rangle$ is independent of the external potential and, thus, forms an universal functional for all the N-electron systems. Clearly, the exact form of the $F[n]$ is unknown and approximations are needed. The very first density-functional method is called Thomas-Fermi theory, in which the interaction energy is approximated by the Hartree energy of the electron charge distribution and, for the kinetic energy, a local approximation is used [1]. The results of Thomas-Fermi theory are seldom satisfactory and, therefore, more elaborate approximations and methods have been developed.

The formulation of the DFT by Hohenberg and Kohn restricts to the nondegenerate ground states and to v-representable densities that must be in one-to-one relation to the external potential. The constrained search formulation of the original Hohenberg-Kohn theorem by Levy [18] and Lieb [19] relieves these restrictions. Levy showed that it is in fact sufficient to constrain the search for the (possibly degenerate) ground state to the N-representable densities that result from square-integrable, antisymmetric wave functions.

2.2 The Kohn-Sham Method

Kohn and Sham turned the density-functional theory into a widely-used tool in computational condensed matter physics. The original idea is to examine a non-interacting reference system for which the density is exactly the ground state density $n(\boldsymbol{r})$ [20]. By introducing the exchange-correlation functional, the many-electron problem reduces to a set of single-electron equations, describing an individual electron moving in an effective potential created by all the others.

Non-interacting reference system

The Hamiltonian for a system where all the interactions are turned off is simply a sum of one-body operators, that is,

$$H_s = \sum_{i=1}^{N} h_i = \sum_{i=1}^{N} \left(-\frac{\hbar^2}{2m^*} \nabla_i^2 + v_s(\boldsymbol{r}_i) \right), \tag{2.3}$$

where $v_s(\boldsymbol{r})$ is a single-particle potential. The wave function is a Slater determinant constructed from the N lowest one-electron states ψ_i satisfying equation $h\psi_i = \varepsilon_i\psi_i$. The density of the Slater determinant is simply a sum of the densities of the one-electron orbitals. The resulting functional for the energy of the non-interacting system is

$$E_s[n] = T_s[n] + V_s[n] = \sum_i \langle\psi_i| - \frac{\hbar^2}{2m^*}\nabla^2|\psi_i\rangle + \int v_s(\boldsymbol{r})n(\boldsymbol{r})\mathrm{d}\boldsymbol{r}. \tag{2.4}$$

Minimisation of the above functional leads to Euler-Lagrange equation

$$\mu = v_s(\boldsymbol{r}) + \frac{\delta T_s[n]}{\delta n(\boldsymbol{r})}, \tag{2.5}$$

where the Lagrange multiplier μ is needed for conservation of the electron number. Kohn and Sham used these features of the non-interacting system to reduce the interacting many-body problem into a set of one-body equations.

Kohn-Sham equations

In the Kohn-Sham method, the exact kinetic energy is replaced by the non-interacting kinetic energy T_s. Furthermore, the main contribution to the interaction energy is contained in the electrostatic Hartree energy,

$$U[n] = \frac{1}{2}\int \mathrm{d}\boldsymbol{r}\int \mathrm{d}\boldsymbol{r}'\frac{e^2 n(\boldsymbol{r})n(\boldsymbol{r}')}{4\pi\epsilon\epsilon_0|\boldsymbol{r}-\boldsymbol{r}'|}. \tag{2.6}$$

In order to produce the desired separation into $T_s[n]$ and $U[n]$, the universal functional is written in the form

$$F[n] = T_s[n] + U[n] + E_{xc}[n], \tag{2.7}$$

where the exchange-correlation functional $E_{xc}[n] = T[n] - T_s[n] + U_{ee}[n] - U[n]$ contains the difference between the true kinetic energy and non-interacting kinetic energy and the non-classical part of interaction energy. Using these definitions, the Euler-Lagrange equations for the non-interacting reference system (2.5) and for the true interacting system become identical if we identify v_s as

$$v_s =: v_{eff}(\boldsymbol{r}) = v_{ext}(\boldsymbol{r}) + \int \frac{e^2 n(\boldsymbol{r})}{4\pi\epsilon\epsilon_0|\boldsymbol{r}-\boldsymbol{r}'|}\mathrm{d}\boldsymbol{r}' + v_{xc}(\boldsymbol{r}), \tag{2.8}$$

where $v_{xc} = \delta E_{xc}/\delta n(\boldsymbol{r})$ is the exchange-correlation potential. This similarity between the reference system and the true system allows us to use the one-body tools to solve the interacting system: For a given v_{eff}, one obtains $n(\boldsymbol{r})$ that satisfies the Euler-Lagrange equation simply by solving the N one-body equations

$$\left\{-\frac{\hbar^2}{2m^*}\nabla^2 + v_{eff}(\boldsymbol{r})\right\}\psi_i(\boldsymbol{r}) = \varepsilon_i\psi_i(\boldsymbol{r}) \tag{2.9}$$

and setting

$$n(\boldsymbol{r}) = \sum_{i=1}^{N} |\psi_i(\boldsymbol{r})|^2. \tag{2.10}$$

The Kohn-Sham energies ε_i and eigenfunctions $\psi_i(\boldsymbol{r})$ do not have a direct physical interpretation, but are more or less mathematical auxiliaries. Nevertheless, they are used to determine bandstructures for lattices, and they give useful information about the internal electronic structure of quantum dots. The equations (2.9) are coupled together via the effective potential (2.8) making solving the ground state density (2.10) an iterative process.

Extensions of DFT to Magnetic Systems

Initially, the DFT was developed in spin-independent formalism. Studies of systems in an external magnetic field, however, call for inclusion of the spin degree of freedom. Spin effects are essential also in the absence of external magnetic fields, for example in open-shell quantum dots [16] and lattices with broken spin symmetry (such as ferromagnets).

The spin polarization effects are included in spin-density-functional theory (SDFT) introduced by von Barth and Hedin [21]. In the SDFT, the total electron density comprises of spin-up and spin-down densities, that is, $n = n_\uparrow + n_\downarrow$, where

$$n_\sigma(\boldsymbol{r}) = \sum_{i=1}^{N_\sigma} |\psi_{i\sigma}(\boldsymbol{r})|^2 \tag{2.11}$$

for N_σ electrons with spin $\sigma = (\uparrow, \downarrow)$. Consequently, there are now two sets of Kohn-Sham equations with orbitals $\psi_{i\sigma}(\boldsymbol{r})$ and energies $\varepsilon_{i\sigma}$, one for each spin. The effective potential (2.8) becomes spin-dependent, as the exchange-correlation potential is spin-dependent, that is, $v_{xc}^\sigma = \delta E_{xc}/\delta n_\sigma(\boldsymbol{r})$. In the presence of magnetic field, there is also a spin-dependent Zeeman term as the field couples to the electron spin.

The contribution of electronic currents to the energy functional are neglected in the SDFT, although magnetic field couples to the physical (gauge-invariant) current density that consists of paramagnetic and diamagnetic current densities. At high magnetic fields this coupling cannot be ignored and, therefore, Vignale and Rasolt constructed so-called current-spin-density-functional theory (CSDFT) [22], where the basic variables are the paramagnetic current density $\boldsymbol{j}_p(\boldsymbol{r})$ and the spin densities $n_\uparrow$ and $n_\downarrow$.

Local density approximation for the exchange-correlation energy

Formally, the Kohn-Sham method is an *exact* method for finding the ground state. However, the exact form of exchange-correlation energy is unknown, and one must resort to approximations. For two- and three-dimensional systems, the simplest approximation is local (spin) density approximation (LSDA), which assumes electron density to be locally homogenous in an infinitesimal volume-element. The total exchange-correlation energy is obtained by integrating over the elements,

$$E_{xc}^{LDA}[n] = \int n(\boldsymbol{r})\varepsilon_{xc}(n)\mathrm{d}\boldsymbol{r}. \tag{2.12}$$

Here $\varepsilon_{xc}(n)$ is the exchange-correlation energy per particle in an uniform electron gas of density n. An alternative measure of density is given by the density parameter (Wigner-Seitz radius) r_s, which is $r_s = 1/\sqrt{\pi n}$ for two-dimensional gas. Despite the raggedness of the local approximation, it works surprisingly well also for atomic systems [23].

The exchange-correlation energy of the uniform electron gas (also called *jellium* in the literature) can be divided into exchange and correlation parts, $\varepsilon_{xc} = \varepsilon_x + \varepsilon_c$. The exchange part is obtained by calculating the exchange energy of the uniform gas using the Hartree-Fock theory [1]. However, an analytic expression for the correlation energy of the uniform gas is known only in extreme limits. At high densities ($r_s \to 0$), the interaction part of the jellium Hamiltonian can be treated as a perturbation and, consequently, the correlation energy can be obtained from many-body perturbation theory [24, 2]. At low density ($r_s \to \infty$), the uniform liquid phase becomes unstable against the formation of a close-packed Wigner lattice of localised electrons. Since the Coulomb interaction gives the dominant part of the total energy at low densities, the correlation energy can be approximated from the Madelung electrostatic and zero-point vibrational energies of the Wigner lattice.

For a local approximation in the SDFT, one needs spin-resolved exchange-correlation energy $\varepsilon_{xc}(n,\xi)$ for arbitrary relative spin polarisation $\xi = (n_\uparrow - n_\downarrow)/n$. A standard practice is to assume that the polarisation dependence of $\varepsilon_{xc}(n,\xi)$ follows that of the pure exchange energy [21]. Then

$$\varepsilon_{xc}(n,\xi) = \varepsilon_{xc}(n,0) + f(\xi)[\varepsilon_{xc}(n,1) - \varepsilon_{xc}(n,0)], \tag{2.13}$$

where the polarisation dependence $f(\xi)$ interpolates between the fully polarised ($\xi = 1$) and the unpolarised ($\xi = 0$) limits. Another representation for the electron gas is provided by Perdew and Wang [25], and similar forms are used also for two-dimensional electron gas. We shall discuss these in detail later on.

The various representations of the correlation energy interpolate between the exactly known high-density and low-density limits. At intermediate densities, they are fitted to correlation energy data obtained from quantum Monte Carlo simulations of homogenous electron gas.

2.3 Numerics: Plane Wave Technique

The uppermost benefits of the Kohn-Sham method are its flexibility and easy implementation for computations. There are several approaches to the numerical solution of the Kohn-Sham equations. One branch uses real-space methods based on finite differences or finite elements where the values of the Kohn-Sham orbitals $\psi_{i\sigma}(\boldsymbol{r})$ are solved directly in a mesh inside the computing region [26]. Heiskanen *et al.* introduced a real-space multigrid method where the eigenvalues are solved by minimising the Rayleigh quotient and the error reduction rate of the solution is accelerated by using cycles of coarse and fine grids [27].

Plane Waves

A conventional approach is to expand the orbitals $\psi_{i\sigma}(\boldsymbol{r})$ in a complete set of functions and diagonalise the subsequent matrix of the Kohn-Sham Hamiltonian. In our model for quantum dots a reasonable choice could be the single-particle basis (1.3). Particularly, it is used in Kohn-Sham calculations with circularly symmetric effective potential. We do not impose symmetry restrictions but choose plane wave basis for which we can use efficient fast Fourier algorithms. In order to solve the coupled set of one-electron equations (2.9), we expand the states in a finite set of plane waves by writing

$$\psi_{i\sigma}(\boldsymbol{r}) = \frac{1}{\sqrt{V}} \sum_{\boldsymbol{k}} C_{\boldsymbol{k}}^{i\sigma} \exp(i\boldsymbol{k} \cdot \boldsymbol{r}), \tag{2.14}$$

where $\boldsymbol{k} = 2\pi(\frac{n_1}{L_x}, \frac{n_2}{L_y})$ with integers n_i ranging from $-n_i^{cut}$ to n_i^{cut}. To describe the densities and other quantities in the real-space, the rectangular calculation box of area $V = L_x L_y$ is divided into a mesh of $(4n_1^{cut}+1) \times (4n_2^{cut}+1)$ equidistant points. Typical values used for the plane wave cut-offs n_i^{cut} are 8 and 11 giving a total of $17 \cdot 17 = 289$ to $23 \cdot 23 = 529$ plane waves.

By using the expansion (2.14) in the equations (2.9), we get a matrix equation

$$\sum_{\boldsymbol{k}} \left\{ \frac{\hbar^2 k^2}{2m^*} \delta_{\boldsymbol{k},\boldsymbol{k}'} + V_{\boldsymbol{k},\boldsymbol{k}'}^{eff} \right\} C_{\boldsymbol{k}}^{i\sigma} = \varepsilon_{i\sigma} C_{\boldsymbol{k}'}^{i\sigma}, \tag{2.15}$$

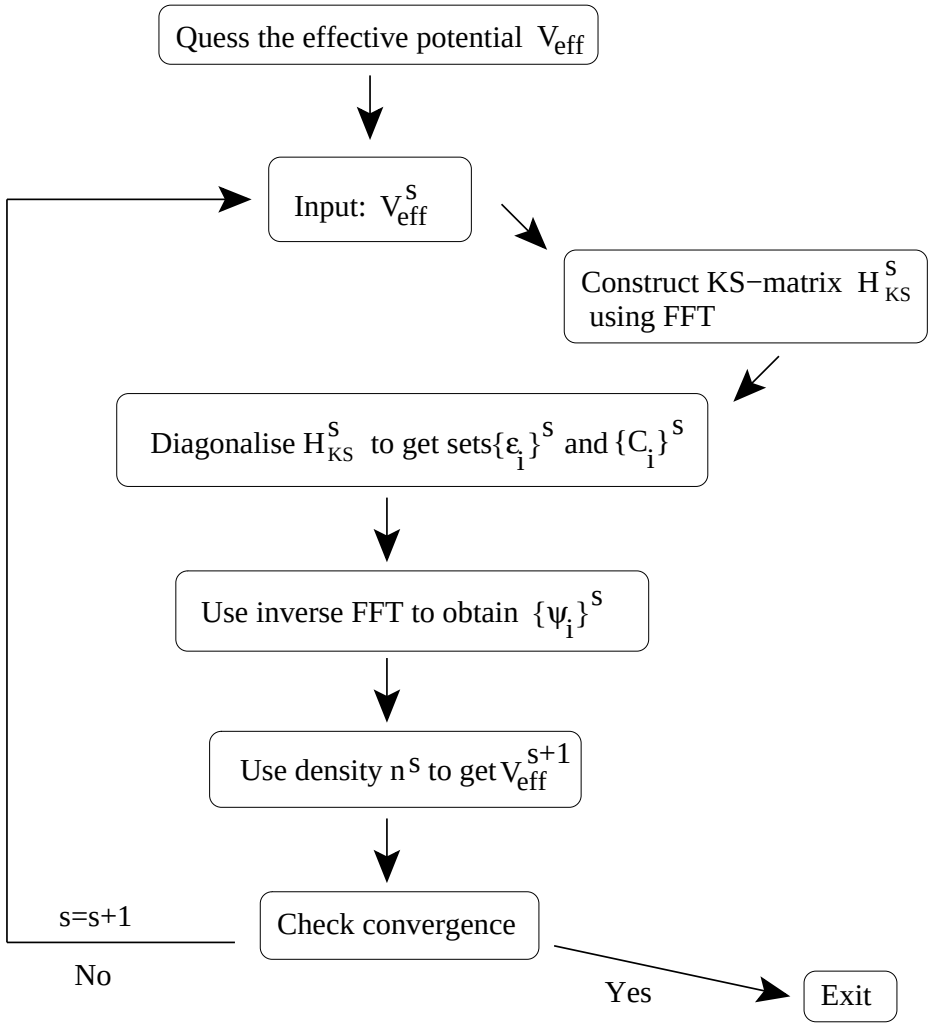

Figure 2.1: Flow chart of the iteration step s in the self-consistent solution of the Kohn-Sham equations

where $V^{eff}_{\boldsymbol{k},\boldsymbol{k}'} = V^{eff}_{\boldsymbol{k}-\boldsymbol{k}'}$ is the Fourier component of the effective potential (2.8).

Figure 2.1 shows a flow chart for the self-consistent solution of the Kohn-Sham equations. Iterations are started from an initial guess of the effective potential for both spins. Usually, calculations are performed with several different initial guesses with small random perturbations added in order to avoid convergence into the local minima of the potential surface. The Fourier components of the effective potential are computed with the fast Fourier transformation and the Hamiltonian matrix is diagonalised giving the lowest eigenenergies $\varepsilon_{i\sigma}$ and the corresponding eigenvectors $\boldsymbol{C}^{i\sigma}$. Inverse fast Fourier transformation computes the real-space eigenfunctions through equation (2.14) after which the density and the new effective potential can be obtained. This process is repeated until self-consistency is achieved, in other words,

when the effective potential does not change anymore. For a better convergence, new potential is mixed with the old one through $v_{eff}^{new} = (1-\alpha)v_{eff}^{old} + \alpha v_{eff}^{new}$ with α ranging from 0.01 to 0.1.

2.4 Other Approaches

Despite the evident benefits of the local density KS-method, there are well-justified doubts whether a method with a mean-field flavour can give a full account of the many-body effects in quantum dots. These issues become increasingly important in the studies of strongly correlated low-density quantum dots that deviate significantly from a uniform system, whereupon the local approximation for correlation is expected to fail.

Exact Diagonalization

A straightforward way to solve few-electron correlated states in a quantum dot is to use exact diagonalization of the many-body Hamiltonian matrix [4]. In quantum chemistry the exact diagonalization is known as the configuration interaction method [5] and it is also used in the shell model calculations of nuclear physics [6]. The basic idea is to construct a Hamiltonian matrix of operator (1.1) and to diagonalise it. The matrix elements are calculated between Slater determinants (or Fock states in the occupation number representation) built up of different configurations of single-particle states. Suitable choice for the basis in the model Hamiltonian would be the basis (1.3). By increasing the number of configurations, the lowest eigenvalue converges practically to the exact ground state energy and, without any extra cost, the whole excitation spectrum is obtained. Furthermore, very accurate many-body wave functions with correct correlations are obtained.

The applicability of this seemingly unbeatable method breaks down with increasing electron number and decreasing density because the number of configurations needed for convergence grows rapidly. Computation becomes slightly easier when symmetries of the problem are used to reduce the dimension of the configuration space. For example, in studies of circular quantum dots we may do the diagonalization for a fixed total angular momentum, and in strong magnetic fields we may truncate the single-particle basis to the lowest Landau levels. Despite these facilitations, the maximum number of electrons is limited to around ten [30].

Quantum Monte Carlo

Another group of many-body methods for correlated systems is formed by the quantum Monte Carlo methods that include variational Monte Carlo (VMC), diffusion Monte Carlo (DMC) and path integral Monte Carlo (PIMC) among others (for reviews, see [28] and [29]). These methods can be used to calculate quantum dot ground states even at low densities and for a large number (> 10) of electrons with a good accuracy. A common problem in using quantum Monte Carlo techniques for fermions is to preserve the correct antisymmetry of the wave function.

In the variational Monte Carlo method, the wave function is approximated with a suitable trial function having a set of variational parameters. Monte Carlo integration is used to calculate the many-dimensional integrals, and the parameters in the wave function can be varied to minimise the energy. The accuracy of the VMC is naturally conditional on the choice of the trial wave function and the energy given by it is an upper bound on the ground state energy due to the variational principle. A usual form for the trial wave function is $\Psi = \exp(J)\Psi_S$, where Ψ_S is an antisymmetric Slater determinant or a linear combination of Slater determinants, and $\exp(J)$ is a symmetric Jastrow factor that describes the correlations among particles. A usual form of Jastrow factor is

$$J = \sum_{i=1}^{N} \chi(\boldsymbol{r}_i) - \frac{1}{2} \sum_{i \neq j} u(\boldsymbol{r}_i, \boldsymbol{r}_j), \tag{2.16}$$

where functions χ and u include one- and two-body correlations, respectively.

The fixed-node diffusion Monte Carlo method is a stochastic projector method that maps out the lowest energy state from a trial wave function. This probabilistic algorithm can handle only positive distributions, but the fermion wave functions will take also negative values as a result of antisymmetry in particle exchange. To circumvent this drawback, the DMC algorithms often resort to fixed-node approximation, where the nodal surface of the wave function is fixed to be the same as that of an antisymmetric trial function but no assumptions are made about the functional form between the nodes. Fixed-node DMC algorithm may therefore be regarded as a variational method that gives exact results if the trial nodal surface is exact.

Comparisons of the Methods in Quantum Dot Modelling

Both the exact diagonalization and the quantum Monte Carlo method have been used in quantum dot modelling. the QMC methods are used by several authors to calculate the electronic structures of vertical quantum dots. The obtained addition energies

agree nicely with the measured data and with the LSDA calculations. However, for four-electron dots some DMC and PIMC calculations predict ground state spin $S = 0$ that violates Hund's first rule [61]. The $S = 0$ and $S = 1$ states obtained by Pederiva *et al.* in DMC calculations [31] were nearly degenerate, and in a recent erratum they found $S = 1$ to be the ground state in agreement with Hund's rule [32]. Exact diagonalization gives ground state spin $S = 1$ obeying Hund's rule.

At lowered densities, the electrons in the harmonic confinement are expected to localise into a Wigner molecule, a finite-size counterpart of Wigner lattice. Monte Carlo simulations of classical point-charges in harmonic potential indicate that the electrons arrange themselves into specific geometric configurations. Exact diagonalization [33] and PIMC [34] calculations show that signals from Wigner crystallisation for small number of electrons can be observed already at relatively high density ($r_s \approx 4\ a_0^*$). Localisation in LSDA calculations is hindered by the spurious self-interaction effect arising from the local approximation for the exchange-correlation energy. However, we will see that in quantum dot systems with increased degrees of freedom, such as double-layer dots, the localisation can be seen also in LSDA calculations.

Broken symmetries in the DFT

The Hamiltonian (1.1) preserves orbital angular momentum due to the circular symmetry of the confining potential. Consequently, the density obtained from the exact wave function retains circular symmetry. Despite this, the mean field of the density-functional theory can be deformed in the case of orbital degeneracy or at low densities where the electrons localise into a Wigner molecule. The broken symmetry is directly revealed in the density calculated from the Kohn-Sham orbitals. The question whether this phenomenon is an artifact of the mean field theory or a reflection of the internal structure of the exact wave function is under continuous debate [61].

Broken symmetries are identified by analyzing rotational and vibrational spectra of circular quantum dots [35], quantum rings [36] and nuclei [37]. Deformations are also found to be an universal feature of small alkali-metal clusters and nuclei [38]. Furthermore, an arbitrary rotation of the deformed mean field solution yields an equivalent solution. Therefore, the symmetry-violating mean-field can be viewed as an intrinsic state of the system.

On the other hand, Harju *et al.* have addressed the problem of *ensemble v-representability* in the case of rectangular quantum dots [39]. They compared Kohn-Sham densities to the exact densities and found that the mean-field spin density wave solution was in fact a superposition of the ground state singlet and the excited triplet states.

The above arguments suggest that the deformed solutions are not merely artifacts of

the Kohn-Sham mean field, but they must still be examined carefully and critically. Despite these possible pitfalls of the density-functional methods, they give good insight to the qualitative features of the electronic structure and are applicable also to large systems.

3 Vertical Quantum Dot Molecules

Both lateral and vertical quantum dots can be coupled to form "artificial molecules" [40, 41]. Coupling brings forth new degrees of freedom to the quantum dot structure leading to new features in electronic properties. For example, the inter-dot separation and the type of carriers can be varied and, thus, the inter-dot coupling can be tuned at will. In a vertical quantum dot molecule in strongly coupled (quantum mechanical) regime, the electrons delocalise over both dots leading to a splitting between bonding and anti-bonding states. The splitting diminishes approximately exponentially with increasing inter-dot spacing until the isolated dots are only electrostatically coupled [43]. The splitting leads to formation of molecule-type phases [44] and, depending on applied magnetic field, to specific "magic" orbital and spin angular momenta [45].

In publication [I] we examine electronic structure of vertical quantum dot molecules containing electrons and holes. By tuning the external parameters such as the confinement strength and inter-dot separation, the ground state characteristics can be varied. There are two competing mechanisms to resolve degenerate states, namely Hund's rule and Jahn-Teller deformation. Furthermore, at longer inter-dot distances the Coulomb attraction localises the electron-hole pairs.

3.1 Electron-Hole Quantum Dot Molecules

Vertical electron-hole quantum dot molecules can be realised in bipolar heterostructures with separated electron and hole layers in equilibrium. Such heterostructures are, for example, biased GaAs/AlGaAs or InAs/GaSb alloys [46, 47]. The inset of figure 3.1 shows schematically a double layer quantum dot where a two-dimensional quantum dot with electrons is separated by distance z_0 from another dot confining an equal number of holes.

In order to study the double dot with the Kohn-Sham method in the local spin density approximation, we need a set of four coupled equations for the electron and hole spin

densities n^e_σ and n^h_σ. The effective potential for, say, electrons is then given by

$$v^e_{eff,\sigma} = \frac{1}{2}m^*\omega_0^2 r^2 + \int \frac{e^2 n^e(\boldsymbol{r}')}{4\pi\epsilon\epsilon_0|\boldsymbol{r}-\boldsymbol{r}'|}\mathrm{d}\boldsymbol{r}' - \int \frac{e^2 n^h(\boldsymbol{r}')}{4\pi\epsilon\epsilon_0\sqrt{|\boldsymbol{r}-\boldsymbol{r}'|^2+z_0^2}}\mathrm{d}\boldsymbol{r}' + v_{xc,\sigma}(n^e(\boldsymbol{r}),\xi^e(\boldsymbol{r})). \quad (3.1)$$

Here the first term is the external harmonic confinement and the next two terms are the repulsive in-layer and attractive inter-layer Hartree potentials, respectively. For the exchange-correlation potential, we used the von Barth and Hedin formulation of the local exchange-correlation energy (2.13) for both the electron and hole densities. The inter-layer electron-hole correlation is neglected, which is a reasonable approximation for large inter-dot separations and strong external confinements.

In our model, the quantum dots are assumed to be identical so that the harmonic confinements and the effective masses of holes and electrons are the same, that is, $m^*_h = m^*_e = m^*$ and $\omega^e_0 = \omega^h_0 = \omega_0$. Furthermore, the number of electrons is assumed to be the same as the number of holes, that is, $N_e = N_h = N$. Owing to the fact that the dots are identical, the ground state densities of electrons and holes are necessarily identical.

3.2 Ground State Properties

Phase Diagram

Electronic properties of vertical double quantum dots are determined by three parameters: the inter-dot separation z_0, the confinement ω_0 and the number of electrons and holes N. Figure 3.1 shows ground state phases as a function of the inter-dot separation z_0 and the confinement ω_0 for a double quantum dot confining four electrons and four holes. The different ground state spin structures are separated by a line, and a contour plot of typical particle density in each phase is shown. In the case of four electrons and holes, there are two particles in the degenerate p-state of each dot. This degeneracy is lifted either by deformation of the mean-field or by magnetisation according to Hund's first rule.

When both z_0 and ω_0 tend to zero, the electrons and the holes form a plasma droplet. The Kohn-Sham Hamiltonian includes only kinetic and exchange-correlation energies as the Hartree potentials of the electrons and the holes cancel each other. At this "ultimate jellium" limit, the orbital degeneracies of the finite droplets are removed by deforming the mean-field, which leads to Jahn-Teller deformations of the density.

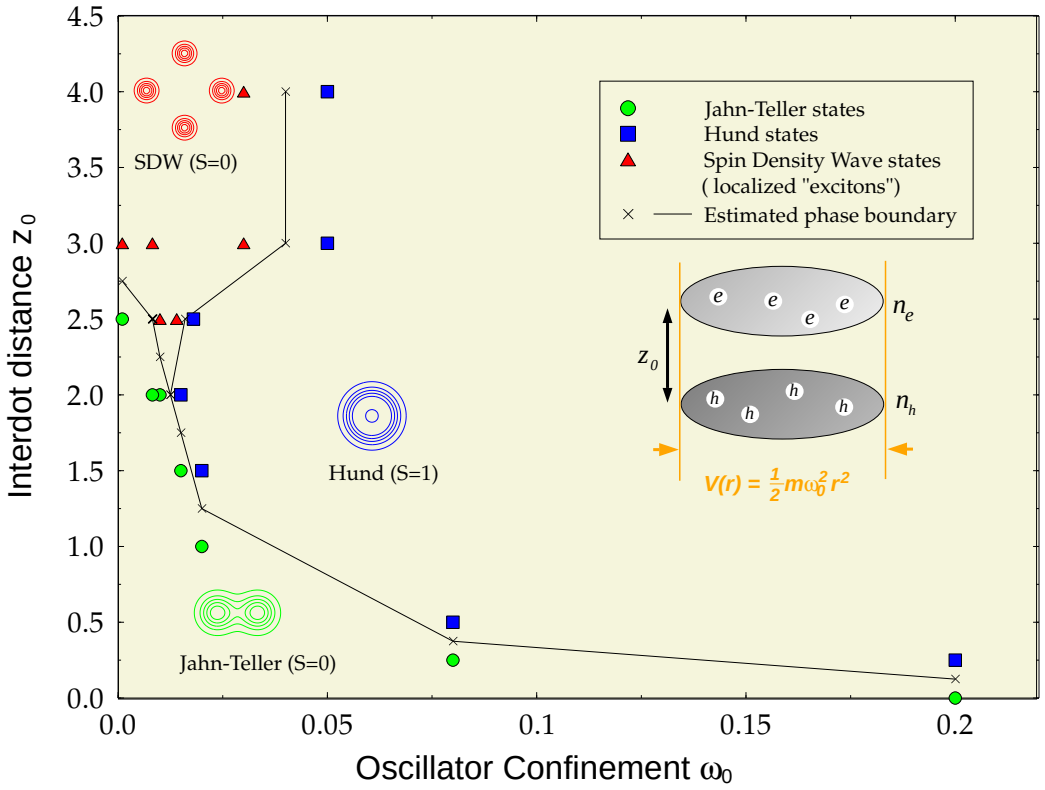

Figure 3.1: Phase diagram of an electron-hole double dot with 4 electrons and 4 holes as a function of confinement ω_0 and inter-dot distance z_0. Estimated phase boundary separates the different spin structures, and a characteristic particle density is shown in each phase. The inset shows a schematic picture of the bipolar quantum dot molecule with electrons e and holes h harmonically confined in two layers separated by distance z_0.

By increasing ω_0 the confinement becomes stiffer forcing the density to azimuthal symmetry. In this case, the degeneracy is resolved by maximising spin according to Hund's rule. At the ultimate jellium limit, that is, when $z_0 = 0.0\ a_0^*$, the deformed ground state persists up to a relatively strong confinement of $\hbar\omega_0 = 1.3$ Ha*.

With small ω_0 and increasing inter-dot separation the particle density in the dots decreases and, eventually, the particles localise into a Wigner molecule. The formation of a Wigner molecule is favoured despite the self-interaction error in the local approximation because the localisation is supported by the attraction between electrons and holes: particles localise on top of each other forming tightly bound electron-hole dipoles (localised excitons). The in-layer correlations lead to antiferromagnetic ordering of spins, however, since there is no inter-layer correlation, the spins between the layers do not couple.

A similar phase diagram is also obtained in the closed shell $N = 6$ case. At the

ultimate jellium limit, the density assumes a triangular deformation and it undergoes a transition to the azimuthally symmetric phase as ω_0 increases. Furthermore, the electrons and holes localise into an antiferromagnetic ring of excitons. We believe that the classical configuration of five particles in a ring with one particle at the center is not favoured because of possible frustration of such a spin arrangement.

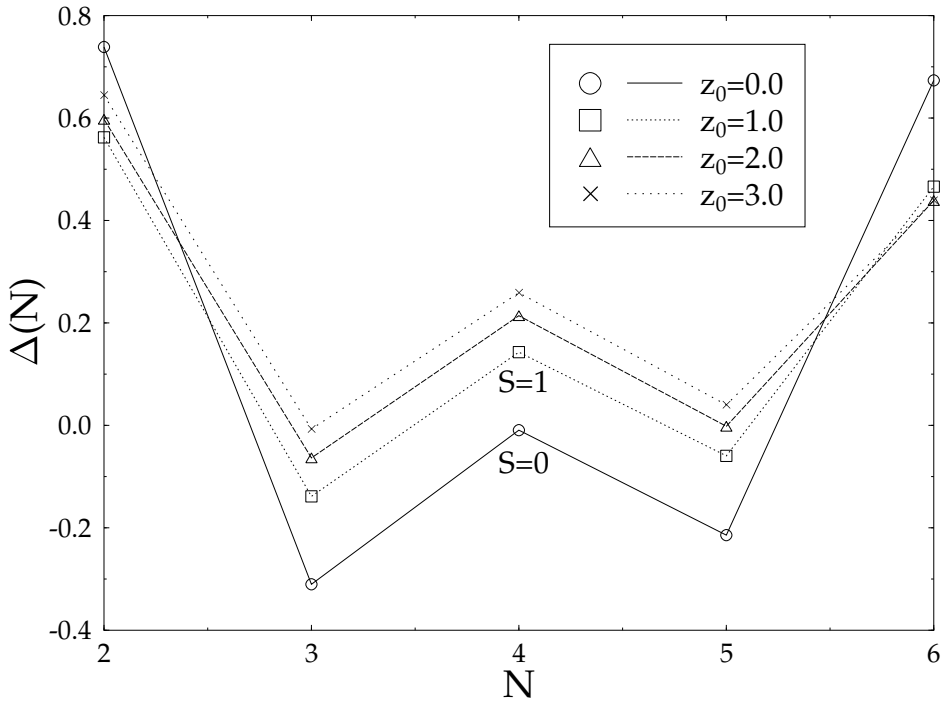

Figure 3.2: Addition energy spectrum for different inter-dot separations z_0. The mid-shell maximum for $z_0 = 0.0\ a_0^*$ is caused by the Jahn-Teller deformation

Addition energies

As was discussed in Section 1.2, measurement of addition energies is an easy way of probing the shell structure of quantum dots. We define the addition energy as the difference in the electrochemical potentials of a bipolar double dot molecule confining $N+1$ and N electrons and holes, that is, $\Delta(N) = E(N+1) - 2E(N) + E(N-1)$, where $E(N)$ is the total energy of the system. The addition energy spectrum of Figure 3.2 shows the closed shell maxima at $N = 2$ and 6. Furthermore, for $z_0 > 0.0\ a_0^*$, the mid-shell $N = 4$ maximum results from spin alignment. At the limit of plasma droplet, the Jahn-Teller deformation is strongest at $N = 4$ leading also to a maximum in the spectrum.

4 Multicomponent Quantum Dots

In the previous chapter, we studied electron-hole bilayer quantum dots using the Kohn-Sham method in the local spin density approximation. The electron-hole correlation was neglected altogether. The inter-layer correlation is usually neglected also in the DFT studies of electronic quantum dot molecules [44]. However, a proper treatment of layered systems should include the inter-layer correlations between the two dots.

Electrons or holes in a quantum dot can originate from different bands of semiconductor. For example, silicon layer has four equivalent conduction electron pockets with anisotropic transverse and longitudinal effective masses. Alternatively, the carriers in a hole inversion layer might originate from heavy and light hole bands that are degenerate at the top of the valence band. As an approximation, the different carriers in the quantum dot could be treated as different species of fermions. Therefore, we make a straightforward generalisation of the SDFT and treat the species as different isospin states of an electron. Consequently, there is one set of orbitals for each component in the Kohn-Sham description.

Non-adiabatic atomic clusters or molecules are yet another example of *multicomponent* systems. If the adiabatic Born-Oppenheimer approximation fails to disrobe the motion of atomic nuclei, both the nuclear and electronic degrees of freedom must be incorporated in the density-functional theory [8].

In publication [II] we develop a multicomponent density-functional theory to treat two-dimensional systems made of mutually interacting but different kinds of fermions. For a local approximation for the exchange-correlation potential, we extend an existing exchange-correlation energy functional to the multicomponent case. In publication [III] we study the electronic properties of multicomponent quantum dots. We assume an effective mass approximation where the band structure effects of the different components are put into single parameter m^*. However, each component may have a mass of its own.

4.1 Two-dimensional Multicomponent Fermion Gas

We estimate the exchange-correlation energy of a multicomponent two-dimensional electron gas to be used in the local density approximation of density-functional cal-

culations of systems with multiple internal degrees of freedom. We call the different degrees of freedom as components. For example, the conventional electron gas will be a two-component electron gas with spin up and spin down electrons being the components. Polarised electrons form in turn a one-component system. First, we derive the Hartree-Fock energy of two-dimensional multicomponent gas. Then, we extend an existing two-component correlation energy function by Attaccalite *et al.* [49] to the multicomponent case.

Exchange-correlation Energy

We consider a homogenous gas consisting of Γ different components. Then $\Gamma = 2$ corresponds to the normal electron gas and $\Gamma = 1$ to the fully polarised ("spinless") gas. The total density of the gas is a sum of the densities of the different components, that is,

$$n = \sum_{i=1}^{\Gamma} n_i = n \sum_{i=1}^{\Gamma} \nu_i, \tag{4.1}$$

where n_i is the density and $\nu_i = n_i/n$ is the dimensionless concentration of component i. The Hartree-Fock energy of the multicomponent gas can be calculated in a similar fashion as that of the two-component gas [7, 1], only now the spin index is generalised to a component index taking Γ different values. Instead of going through the Hartree-Fock algebra, we will take a short-cut and use the fact that, for a homogenous system, the local density approximation for the exchange energy will give the exact result. Exchange energy per particle for component i is $\varepsilon_x^i = -\frac{e^2}{4\pi\epsilon\epsilon_0}\frac{8\sqrt{\pi}}{3\pi} n_i^{1/2}$. The total exchange energy per particle is then

$$\begin{aligned} \varepsilon_x = E_x/N = \frac{1}{N}\sum_{i=1}^{\Gamma} \int \varepsilon_x^i n_i \mathrm{d}\boldsymbol{r} &= -\frac{e^2}{4\pi\epsilon\epsilon_0}\frac{8\sqrt{\pi}}{3\pi} n^{1/2} \sum_i \left(\frac{n_i}{n}\right)^{3/2} \\ &= -\frac{e^2}{4\pi\epsilon\epsilon_0}\frac{8}{3\pi r_s}\sum_i \nu_i^{3/2}. \end{aligned} \tag{4.2}$$

Here, we have used the definition of the two-dimensional density parameter, $n^{1/2} = 1/\sqrt{\pi} r_s$.

The total kinetic energy is the sum of the kinetic energies of the different components, that is,

$$E_k = \sum_{i=1}^{\Gamma} \sum_{\boldsymbol{k}_i} \frac{\hbar^2 k_i^2}{2m_i} = \sum_i \frac{V}{(2\pi)^2} \int\limits_{k_i \le k_{F,i}} \frac{\hbar^2 k_i^2}{2m_i} \mathrm{d}\boldsymbol{k}_i = \sum_i \frac{V\hbar^2}{16\pi m_i} k_{F,i}^4, \tag{4.3}$$

where m_i is the mass of component i. By inserting the radius of the Fermi-disk of the ith component, $k_{F,i} = \sqrt{4\pi n_i}$, we find the total kinetic energy per particle to be

$$\varepsilon_k = E_k/N = \sum_i \frac{V}{N}\frac{\hbar^2\pi n_i^2}{m_i} = \sum_i \frac{\hbar^2\pi(n\nu_i)^2}{nm_i} = \frac{\hbar^2}{r_s^2}\sum_i \frac{\nu_i^2}{m_i}. \tag{4.4}$$

The correlation energy per particle is given by the residual energy that is not included in the Hartree-Fock energy, thus, $\varepsilon_c = \varepsilon_{tot} - (\varepsilon_k + \varepsilon_x)$. We note that the exchange energy is independent of the masses of the components, but the correlation and kinetic energies depend on them and, for the exchange-correlation energy per particle, we then have $\varepsilon_{xc} = \varepsilon_{xc}(r_s, \{\nu_i\}, \{m_i\})$.

A reasonable first approximation for the mass dependence is given by a simple scaling of the exchange-correlation energy. In order to deduce the suitable relation, let us first introduce dimensionless quantities $Z_\gamma = \sum_{i=1}^{\Gamma} \nu_i^\gamma$. Then, by defining an average total mass M via

$$\frac{1}{M} = \frac{1}{Z_2}\sum_i \frac{\nu_i^2}{m_i}, \tag{4.5}$$

we may write the kinetic energy as $\hbar^2 Z_2/r_s^2 M$. By dividing the Hartree-Fock energy by the average mass, we have

$$\frac{\varepsilon_{HF}}{M} = \frac{\varepsilon_k}{M} + \frac{\varepsilon_x}{M} = \frac{\hbar^2 Z_2}{(Mr_s)^2} - \frac{e^2}{4\pi\epsilon\epsilon_0}\frac{8Z_{3/2}}{3\pi(Mr_s)}. \tag{4.6}$$

Thus, the average mass M scales the density parameter r_s. As an approximation, we expect the correlation energy to follow this same scaling and, for the mass dependence of the exchange-correlation energy, we adopt formula

$$\varepsilon_{xc}(r_s, \{\nu_i\}, \{m_i\}) = \frac{M}{m_e}\varepsilon_{xc}(Mr_s, \{\nu_i\}, \{m_i = m_e\}), \tag{4.7}$$

where m_e is the bare electron mass. Finally, we note that at low densities when $r_s \to \infty$ the homogenous multicomponent gas approaches the Wigner crystal limit, where the correlation is dominated by the electrostatic repulsion between the localised particles and, thereby, the masses of the components do not play an important role.

Extension of the Two-component Function

Attaccalite *et al.* [49] parametrised the exchange-correlation energy of the two-dimensional two-component electron gas by fitting an appropriate function to their fixed-node diffusion quantum Monte Carlo calculations. For the exchange-correlation function, they generalised a functional form introduced by Perdew-Wang [25] to the two-dimensional case. The function encompasses the known high and low density limits.

The parametrisation by Attaccalite *et al.* can be written in terms of numbers Z_γ. For a two-component gas we have $\xi = \nu_1 - \nu_2$ and $\nu_1 + \nu_2 = 1$. By squaring them, we find $\xi^2 = 2(\nu_1^2 + \nu_2^2) - 1 = 2Z_2 - 1$. The exchange-correlation energy function then becomes

$$\varepsilon_{xc}(r_s, Z_2, Z_{3/2}) = e^{-\beta r_s}[\varepsilon_x - \varepsilon_x^{(6)}] + \varepsilon_x^{(6)} + \alpha_0(r_s) + \alpha_1(r_s)(2Z_2 - 1) + \alpha_2(r_s)(2Z_2 - 1)^2, \quad (4.8)$$

where $\varepsilon_x^{(6)} = -4\sqrt{2}[1 + \frac{3}{8}(2Z_2 - 1) + \frac{3}{128}(2Z_2 - 1)^2]/3\pi r_s$. The functions $\alpha_i(r_s)$ are parametrised by Attaccalite *et al.*, who calculated total energies also for intermediate polarisations $\xi = (n_1 - n_2)/n = \nu_1 - \nu_2 \in [0, 1]$ corresponding to $Z_2 \in [0.5, 1]$. Extension to higher number of components means an extrapolation of ε_{xc} to range $Z_2 \in [0, 1]$, where extreme $Z_2 = 0$ corresponds to a situation where all the particles in the gas belong to different components, and at $Z_2 = 1$ there is only one component.

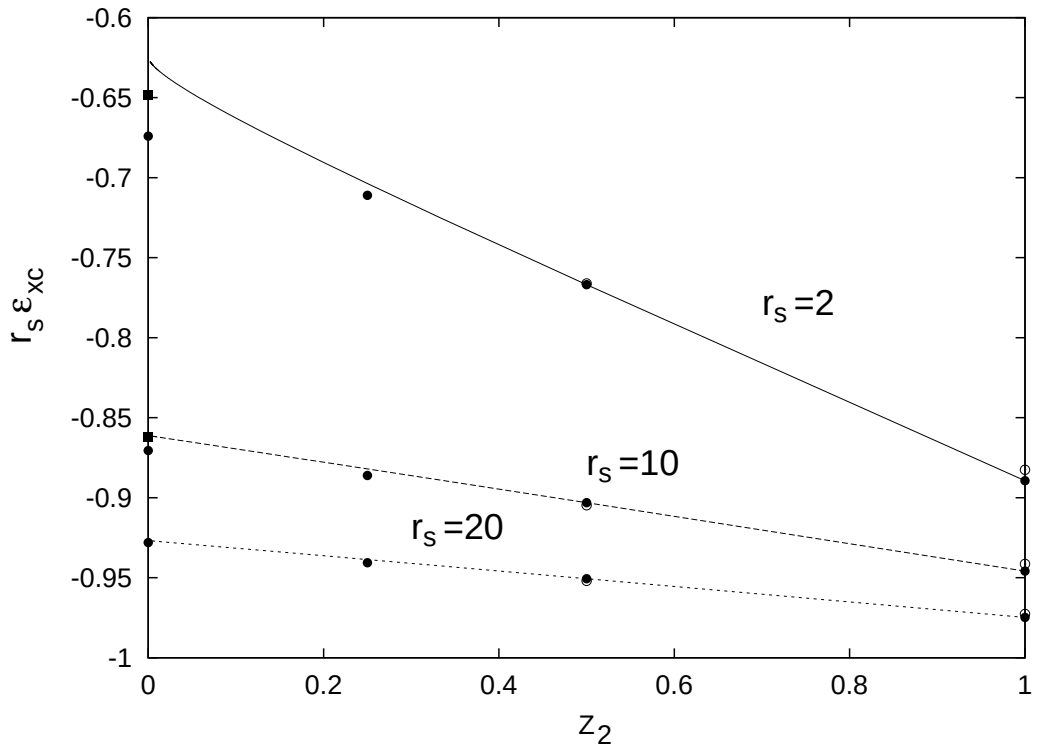

Figure 4.1: Exchange-correlation energy of the multicomponent fermion gas as a function of Z_2. The lines correspond to the extended interpolation function of Eq. (4.8) for different values of r_s, and the points correspond to many-body calculations.

In order to test the extension (4.8), we compared it with the existing many-body calculations. Unfortunately, we found that the available data was scarce. Results are shown

in Figure 4.1, where the lines correspond to the parametrised exchange-correlation energies for different values of r_s and Z_2, and the dots correspond to calculated many-body data. The extended exchange-correlation energy (4.8) reduces exactly to the form of Attaccalite *et al.* in the two-component range $Z_2 \in [0.5, 1]$. For the four-component case, Conti and Senatore [50] presented results for several values of r_s with fixed concentrations, $\nu_1 = \nu_2 = \nu_3 = \nu_4 = 1/4$ corresponding to $Z_2 = 0.25$. Furthermore, we estimated the curious "infinite component" $Z_2 = 0$ limit from the energy of charged Bose gas [51]. Effectively, there is no Pauli exclusion if all the particles belong to different components, since they can be put into different internal "isospin" states. It should be noted, however, that this estimation is only suggestive since the true many-body wave function of the multicomponent fermion system is still anti-symmetric while for bosons it is symmetric. Figure 4.1 shows that the above extended exchange-correlation energy (4.8) fits surprisingly well to the existing data even in the extreme $Z_2 = 0$. Nonetheless, more many-body results in the region $Z_2 < 0.5$ are needed in order to construct a better interpolation function for the multicomponent fermion gas.

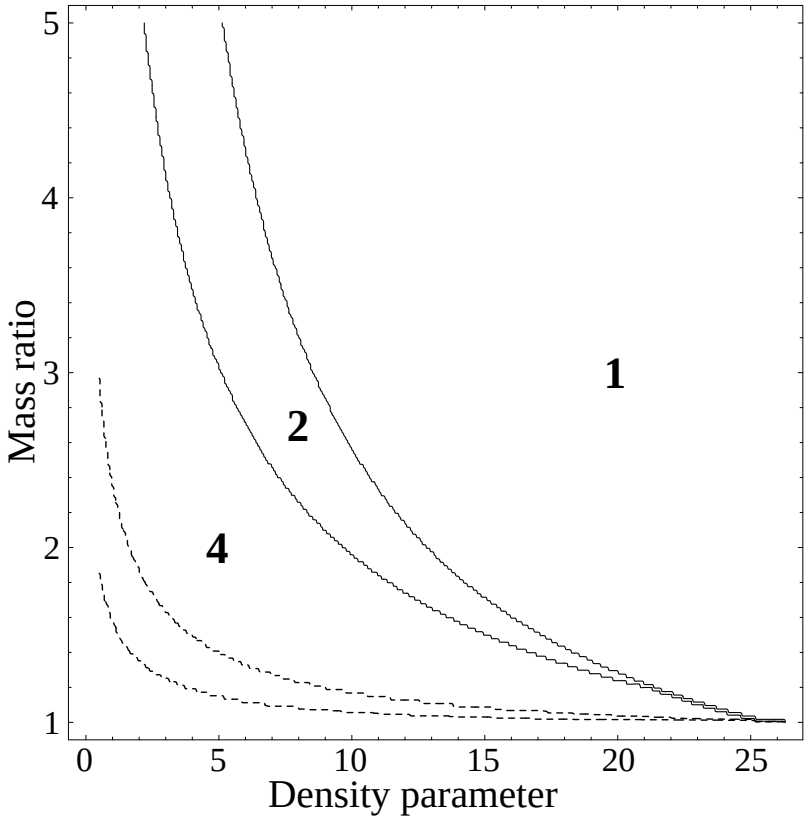

Figure 4.2: Phase diagram for the four-component gas as a function of density parameter r_s and mass ratio $m = m_h/m_l$.

Mass Dependence

The mass difference between the carriers in heterostructures can arise from the different effective masses of materials used in double layer systems or, in hole systems, simply from the effective mass difference between heavy and light hole bands. As discussed in chapter 1, in order to construct a two-dimensional gas from the different components, only the lowest state perpendicular to the 2D plane must be occupied. There can be a constant energy difference between the different components arising from the reduction of kinetic energy of heavier constituents. Therefore, the mass difference and the consequent energy shift should be small enough so that all the components occupy only the lowest perpendicular state allowing the formation of two-dimensional multicomponent gas.

We studied a four-component gas with varying masses at different densities. We fixed the masses to be pairwise equal so that two components are heavier than the other two, that is, $m_1 = m_2 = m_l$ and $m_3 = m_4 = m_h$. Due to the spin degeneracy, there will always be an even number of components, and all pairs of components will have equal masses. Figure 4.2 shows a phase diagram for the four-component gas as a function of density parameter r_s and mass ratio $m = m_h/m_l$ between heavy and light components. For $m = 1$, the concentrations are equal up to $r_s \approx 26.2$ after which there is only one-component present. When increasing m, the kinetic energy and the concentrations of the heavier components decrease and, eventually, the four-component gas goes through the two-component phase down to the polarised one-component phase. Polarisation occurs at smaller r_s as m increases due to the scaling equation (4.7).

4.2 Multicomponent Quantum Dots

The exchange-correlation energy function constructed in the previous section is used in Kohn-Sham density-functional calculations of multicomponent quantum dots. The results are reported in publication [III]. Quantum dots fabricated in multilayer heterostructures, or of multivalley materials are possible realisations of multicomponent nanostructures. For example, in a vertical quantum dot molecule the bonding and antibonding states can be approximated as different components, or as different "isospin" states of an electron. The isospin together with the spin makes the system a four-component quantum dot. In silicon quantum dots, the electrons originate from four (equivalent) valleys of conduction band. As an approximation, we can treat this as an eight component system, where the different valleys and the spin form the components. In addition, the quantum dots made of hole inversion layers will have carriers originating from the light and heavy hole bands.

Multicomponent Kohn-Sham Method

We study a quantum dot containing particles belonging to Γ different components. The generalisation of the standard spin-dependent Kohn-Sham method to multicomponent case is straightforward: There are now Γ coupled equations of form (2.9) that are solved self-consistently. The effective potential for the components $i = 1, 2, \ldots, \Gamma$ consists of external harmonic confinement that is assumed to be the same for all the components, of the repulsive Hartree potential and of exchange-correlation potential $v_{xc,i} = \partial n \varepsilon_{xc} / \partial n_i$ derived from equation (4.8). Thus, the effective potential is given by

$$v_{eff,i} = \frac{1}{2} K r^2 + \int \frac{e^2 n(\boldsymbol{r}')}{4\pi\epsilon\epsilon_0 |\boldsymbol{r} - \boldsymbol{r}'|} \mathrm{d}\boldsymbol{r}' + v_{xc,i}(r_s(\boldsymbol{r}), \{\nu_i(\boldsymbol{r})\}, \{m_i\}), \tag{4.9}$$

where K is the strength of the external confinement. The total density of a system containing $N = N_1 + \ldots + N_\Gamma$ electrons is given by the Kohn-Sham orbitals through equation

$$n(\boldsymbol{r}) = \sum_{i=1}^{\Gamma} \sum_{k=1}^{N_i} |\psi_{i,k}(\boldsymbol{r})|^2. \tag{4.10}$$

The ground-state is found by varying numbers N_i and choosing the combination giving the lowest energy. Otherwise the solution procedure follows the discussion of Section 2.3.

Shell structure

The filling of shells in high-density quantum dots is easily observed from the addition energy spectrum [61]. We studied the addition energy spectrum of an ideal four-component quantum dot at density $r_s = 2.0\ a_0^*$. The degeneracy of the lth shell is now $4l$, which leads to shell closures at $N = 4, 12, 24, \ldots$ corresponding to maxima in the addition spectrum of Figure 4.3. There are smaller maxima at even electron numbers up to 12 electrons and at every third electron number between 12 and 24. These peaks manifest Hund's first rule generalised to the multicomponent case. Exchange energy favors polarisation and, therefore, the degenerate levels are occupied one component at a time to minimise the total energy.

Wigner Molecules

At lowered densities electrons localise into geometric configurations determined by the strong electrostatic repulsion and the external confinement. The localisation in

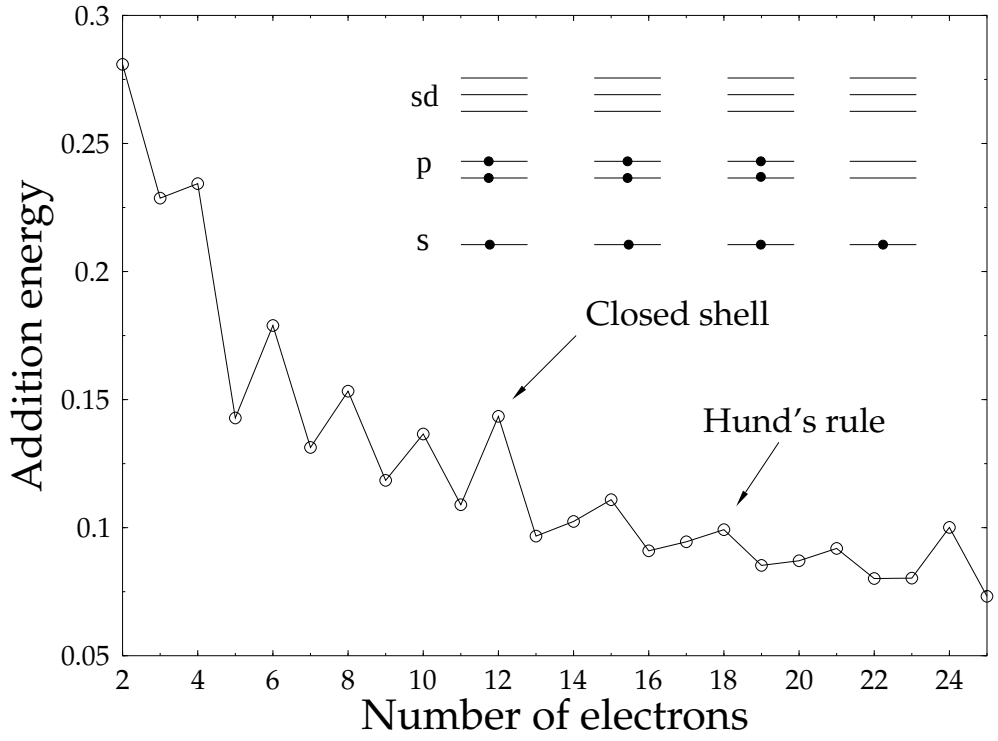

Figure 4.3: Addition energy spectrum of a four-component quantum dot. Electron density corresponds approximately to $r_s \approx 2\ a_0^*$. The inset shows schematically the filling of levels in the case of 10 electrons.

conventional LSDA calculations is hindered by self-interaction but, in the multicomponent systems, the electrons can access more than two internal states, which eases the localisation. Althought the localisation is not complete in the sense that the densities of individual electrons still overlap, the classically predicted geometric configurations are well visible as is shown in the upper panel of Figure 4.4 for 7, 8 and 9 electrons. In 7 and 8 electron Wigner molecules, one electron sits at the center while all the others reside in a ring around the center. In the nine electron case, there are two electrons in the middle and seven in a ring.

We computed addition spectrum shown in the lower panel of Figure 4.4 at low densities for an eight-component system in fixed external confinement with $K = 2 \cdot 10^{-4}$. The spectrum does not show any features of shell structure but merely decreases monotonously due to the capacitive charging of the dot. However, a small kink at $N = 7$ is observed as a precursor of geometric magic configuration, in agreement with the purely classical addition energy spectrum calculated by Bedanov and Peeters [52].

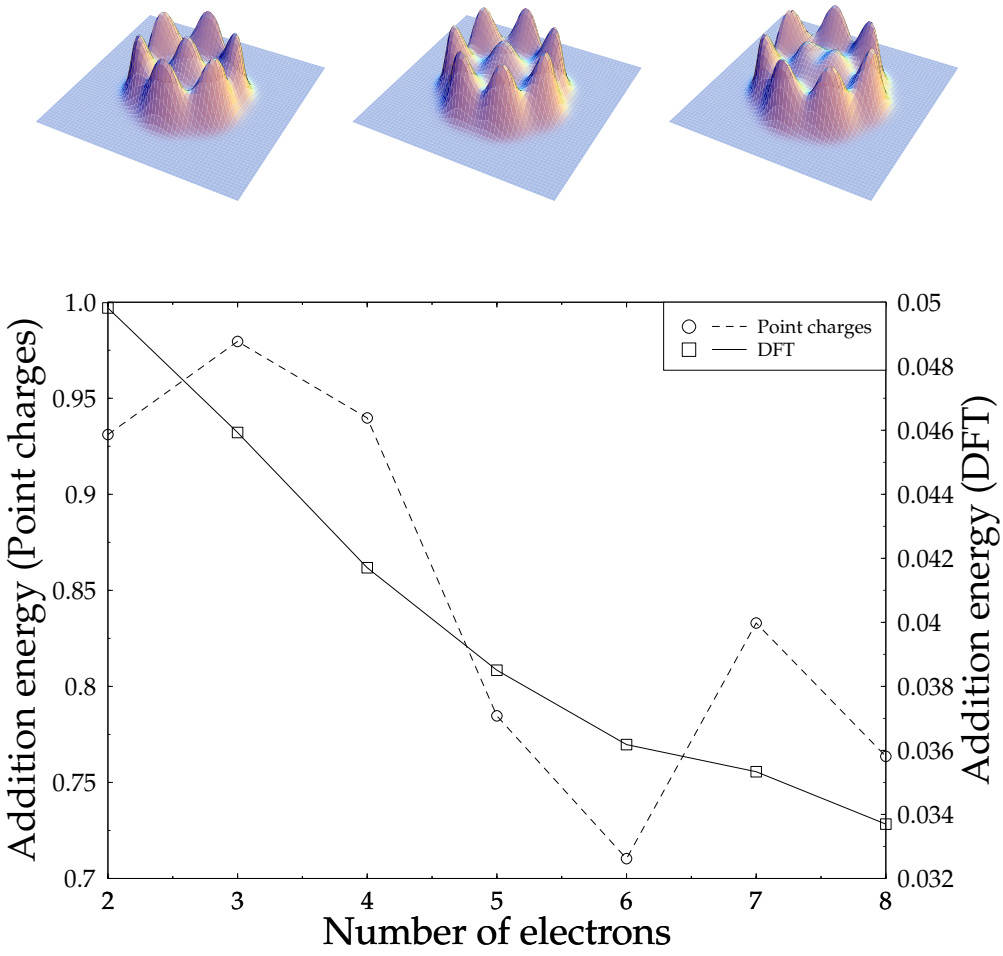

Figure 4.4: Upper: Total electron densities of an eight-component quantum dot having 7, 8 and 9 electrons, respectively, in fixed confinement $K = 2 \cdot 10^{-4}$. Lower: Addition energies for an eight-component quantum dot in fixed confinement $K = 2 \cdot 10^{-4}$. A weak kink at $N = 7$ is a precursor of geometrically magic structure. The addition spectrum of classical point charges is also shown for comparison.

Figure 4.5 shows total densities for a four-component quantum dot with eight electrons at selected values of r_s. At $r_s \lesssim 4\ a_0^*$, density is circular and the ground state is determined by Hund's rule leading to configuration (3,3,1,1). The localisation sets on already at $r_s = 6.0\ a_0^*$ whereupon a Wigner molecule-like state appears. Six electrons reside on the outer circumference with two non-localised in the middle. At $r_s = 14\ a_0^*$, all the electrons are localised and they are distributed spatially so that each electron has neighbours belonging to different components as shown in the contour plot in Figure 4.5.

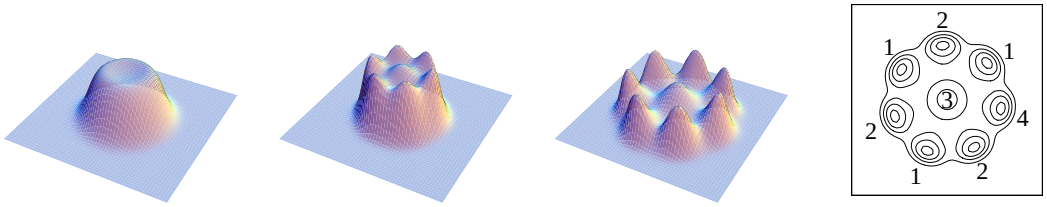

Figure 4.5: Electron densities of a four-component quantum dot for $r_s = 2\ a_0^*, 6\ a_0^*$ and $14\ a_0^*$. The localisation is eased by the fact that the neighbouring localised electrons belong to different components as shown in the contour plot at the left.

Mass Dependence

The effect of varying mass was tested in a four-component dot with $r_s = 2.0\ a_0^*$ and $N = 24$. The mass m of two components was varied while the other two were fixed. Thus, $m_1 = m_2 = m$ and $m_3 = m_4 = 1.0$. For $m = 1.0$, the *sd* shell is filled giving the magic configuration (6,6,6,6). The mass increase shifts the heavier components down in energy due to decreasing kinetic energy as shown in Figure 4.6. At $m = 1.2$, the *sd* orbitals of the light components are empty and heavier *fp* orbitals are occupied according to Hund's rule leading to occupation (10,8,3,3). Already at $m = 1.8$ only two electrons occupy the light component while the heavier components obey Hund's rule with occupation (12,10,1,1).

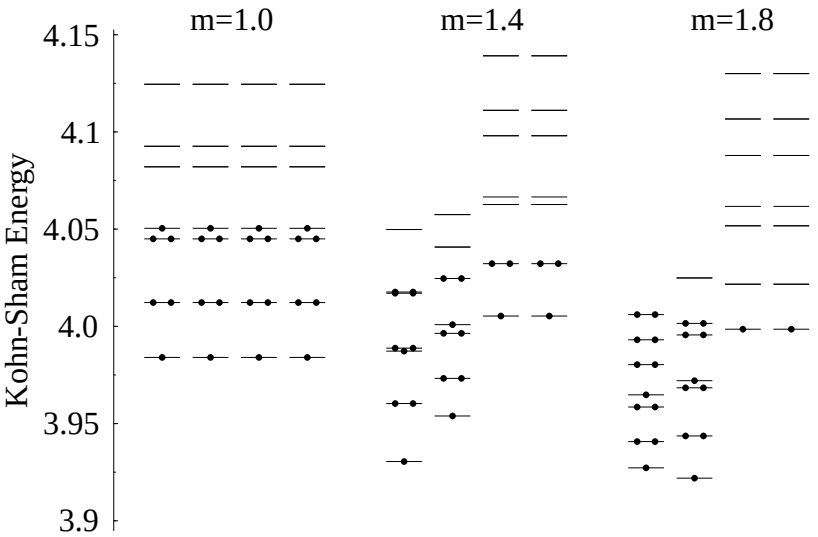

Figure 4.6: Kohn-Sham levels in a four component, 24 electron system with varying effective mass. Light components have mass $m = 1.0$ and heavy mass is indicated in the figure.

5 One-dimensional Quantum Dot Arrays

The intrinsic magnetic properties of nanostructures have drawn much attention due to their potential applicability in spintronics devices [53]. Spontaneous polarisation has been found in one-dimensional quantum point contact constrictions formed in gate-patterned heterostructure [54, 55]. Quantum point contacts [56] and single quantum dots [57] have also spin filtering capabilities, with a possibility to use them for either generating or detecting spin-polarised currents.

Arranging quantum dots in a lattice, one can build artificial crystals with designed band structure, which can be manipulated by tuning the inter-dot coupling and the number of electrons in a unit cell. Experimentally, finite one-dimensional artificial crystals have been fabricated by Kouwenhoven *et al.* [58] already back in 1990. They found conductance oscillations as a function of gate voltage, arising from the mini-band structure of the periodic array. Another interesting artificial array is the Kagome lattice with possible flat-band ferromagnetism [59].

In paper [IV] we study quasi one-dimensional periodic arrays of few-electron quantum dots. We use the standard SDFT without the multicomponent extension. The nearly parabolic confinement for two-dimensional electron gas is provided by a Gaussian-shaped rigid positive background charge distribution. The magnetic and electronic properties depend on the shell filling of the individual quantum dots (electron number per dot N) and on the inter-dot distance (lattice parameter a).

Bloch-Kohn-Sham Method

In order to model the one-dimensional quantum dot array, we consider interacting electrons moving in two dimensions in a rigid periodic background charge distribution en_B. The background charge number per unit cell matches the electronic charge to ensure overall charge neutrality. The Kohn-Sham orbitals are of Bloch form, that is, $\psi_{n\mathbf{k}\sigma}(\mathbf{r}) = \exp(i\mathbf{k}\cdot\mathbf{r})u_{n\mathbf{k}\sigma}(\mathbf{r})$, where n labels the band, $\sigma = (\downarrow, \uparrow)$ is the spin index and the wave vector $\mathbf{k}$ is confined into the first Brillouin zone. The periodic functions

$u_{n\mathbf{k}\sigma}(\mathbf{r})$ satisfy the Bloch-Kohn-Sham equations

$$-\frac{\hbar^2}{2m^*}(\nabla + i\mathbf{k})^2 u_{n\mathbf{k}\sigma}(\mathbf{r}) + v^{\sigma}_{eff}(\mathbf{r}) u_{n\mathbf{k}\sigma}(\mathbf{r}) = \varepsilon_{n\mathbf{k}\sigma} u_{n\mathbf{k}\sigma}(\mathbf{r}), \tag{5.1}$$

where the periodic effective potential is

$$v^{\sigma}_{eff}(\mathbf{r}) = \int \frac{e^2(n(\mathbf{r}') - n_B(\mathbf{r}'))}{4\pi\epsilon_0\epsilon|\mathbf{r} - \mathbf{r}'|} d\mathbf{r}' + v^{\sigma}_{xc}[n(\mathbf{r}), \xi(\mathbf{r})], \tag{5.2}$$

n is the electron density and $\xi = (n_\uparrow - n_\downarrow)/n$ is the polarization. In the local spin-density approximation, we use the form (2.13), parametrised by Tanatar-Ceperley [60], for the polarization-dependent exchange-correlation potential $v^{\sigma}_{xc}[n(\mathbf{r}), \xi(\mathbf{r})]$. In the band structure calculation, the functions $u_{n\mathbf{k}\sigma}(\mathbf{r})$ are expanded in a basis with 11×11 plane waves. Again, the self-consistent solution follows the procedure explained in section 2.3. Iterations are started with anti-ferromagnetic and ferromagnetic initial potentials. In addition, we use an artificial temperature to allow fractional occupation numbers for nearly degenerate states at the Fermi level. The temperature is low enough not to affect the ground-state so the statistical occupations merely help occupying degenerate levels to ensure convergence.

5.1 Magnetism in 1D Quantum Dot Arrays

The confining potential is modelled by a periodic positive background charge distribution described by a sum of Gaussians centered at lattice sites $\mathbf{R} = a(n_x, 0)$, $n_x = 0, 1, 2, \ldots$ Thus, we have

$$\rho_B(\mathbf{r}) = \sum_{\mathbf{R}} \rho_d(\mathbf{r} - \mathbf{R}); \quad \rho_d(\mathbf{r}) = \frac{1}{\pi r_s^2} \exp(-r^2/Nr_s^2), \tag{5.3}$$

where $\mathbf{r} = (x, y)$ is a two-dimensional position vector. A single Gaussian carries positive charge Ne with density $1/\pi r_s^2$ at the center. For the density parameter, we use value $r_s = 2\ a_0^*$. Examples of densities and spin densities in the unit cell are given in Figure 5.1.

The bottom of the confining potential provided by the background charge distribution is harmonic to a good approximation. Studying magnetism in a one-dimensional array, the simplest geometry to choose for the unit cell is a rectangle with two quantum dots per cell. These dots lie in a row along the x axis of the cell, one in the center and one crossing periodically the edge of the cell. In a one-dimensional quantum dot array one can have a smooth transition from the tight-binding description to the nearly-free electron picture simply by varying the lattice constant a.

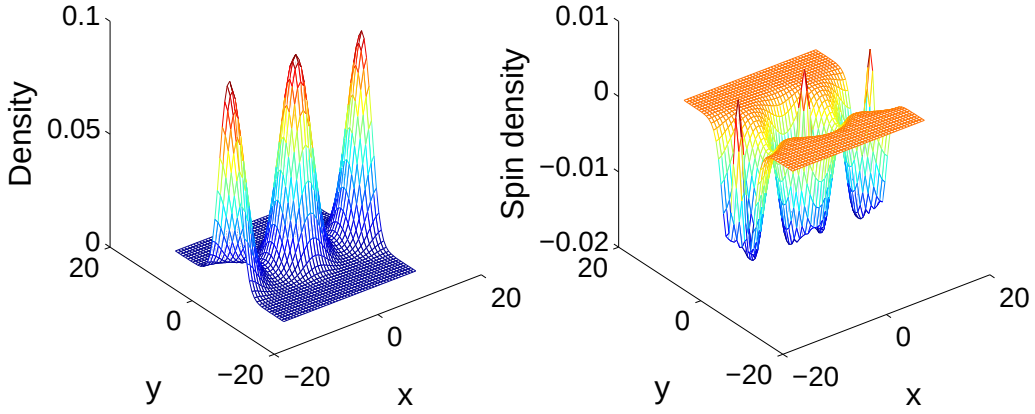

Figure 5.1: Total density and spin density for $N = 3$ at lattice constant $a = 13.05\ a_0^*$.

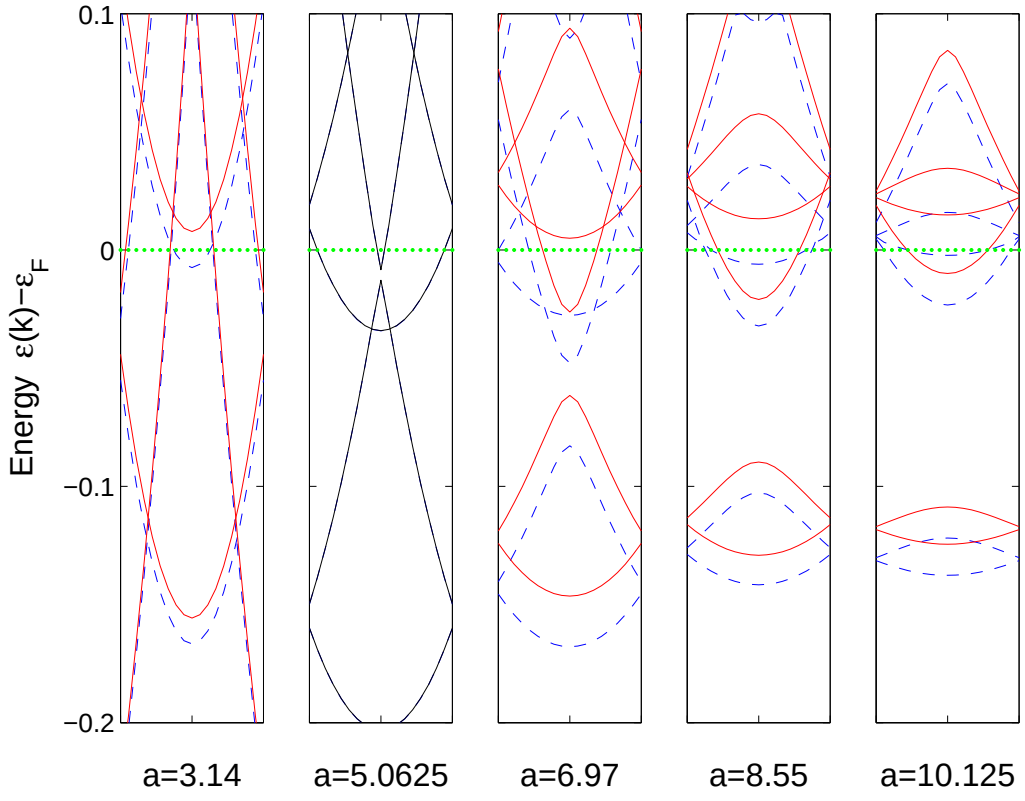

Figure 5.2: Lowest bands at selected values of the lattice constant a for a quantum dot array with three electrons per quantum dot (in atomic units, see text). The spin-down bands are plotted with blue dashed lines, and the spin-up bands correspond to red solid lines. The dotted green line indicates the Fermi-level fixed at zero energy.

Figure 5.2 shows the bands for $N = 3$ at different inter-dot separations. The spin-up and spin-down bands are shown as red solid line and blue dashed line, respectively, and the Fermi-level is fixed at zero energy.

For large values of the lattice parameter a, the electron densities of the individual dots hardly overlap, and the dots are isolated. The bands are flat with band gap energies approximately equal to the single dot level spacings. In this tightly bound extreme the dot array becomes insulating as the hopping probability diminishes with increasing a.

By bringing the quantum dots closer to one another (by decreasing a), the band dispersion increases. Eventually, the band gaps between the tight-binding bands close and the dispersion becomes parabolic. The single quantum dots overlap strongly leading to an essentially homogenous quantum wire with a Gaussian cross-section. In this nearly free limit, the transverse motion of an electron separates from the longitudinal one. The transverse states are quantised by the Gaussian shaped well, while the longitudinal states remain "free" with parabolic dispersion. This is reflected in the band structure, showing nearly equidistant sub-band parabolas. In Figure 5.2 we see that the second transverse sub-band is occupied at $a = 5.0625\ a_0^*$ while at $a = 3.14\ a_0^*$ the Fermi-level reaches the third sub-band.

Shell Filling and Magnetism

The upper panel of Figure 5.3 shows the magnetism of a quasi one-dimensional quantum dot array as a function of electron number per quantum dot and lattice parameter a. The colours indicate regions where the array is conducting (blue) or insulating (yellow). Green corresponds to regions where the Fermi-level resides solely on a single spin band and the arrows indicate the spin arrangement in the array.

For a single electron per quantum dot, $N = 1$, the lowest bonding s-band is filled. Due to the exchange splitting of single dot levels, the bonding and anti-bonding bands are separated by an energy gap and the array shows antiferromagnetic order. The lower panel of Figure 5.3 shows that the spin per dot drops gradually from $1/2$ to 0 as the lattice parameter is decreased and the band gap and the antiferromagnetism persists down to very small values of a. At the closed shell, $N = 2$, both the bonding and anti-bonding 1s bands are full leading to a non-magnetic insulator.

For $N = 3$ and 4, the p-bands are occupied. There are two bonding and two anti-bonding bands for both the spins. The bands with higher dispersion correspond to orbitals with density lobes oriented along the wire. For $N = 3$, there is one p-electron per dot, which triggers ferromagnetism. The bands with majority spin are lower than the ones with minority spin as a result of exchange splitting of the energy bands. The density in the array increases with decreasing a, and at high densities at $a = 5.0625\ a_0^*$

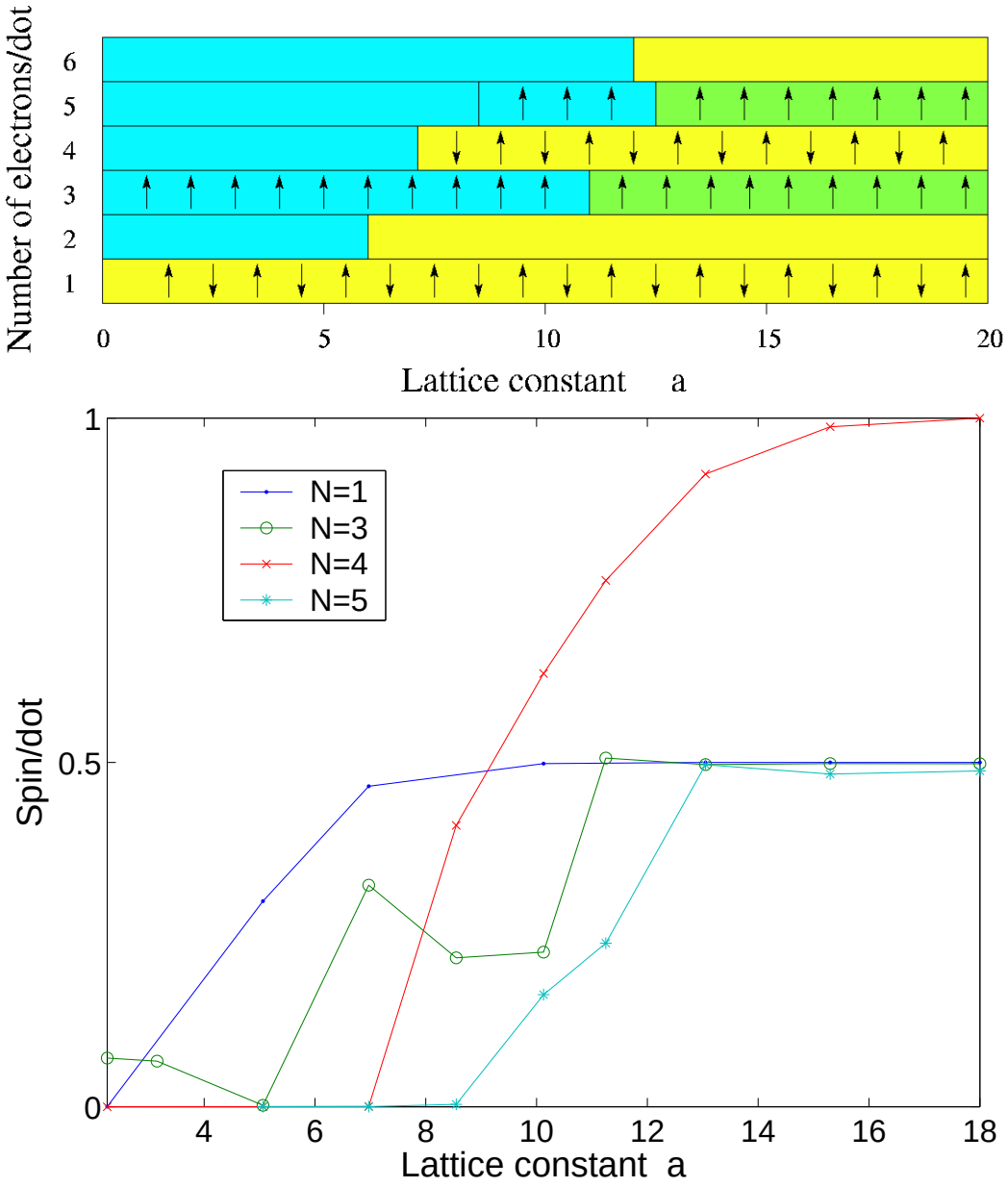

Figure 5.3: Upper: Magnetism in a linear chain of quantum dots as a function of the number of electrons per dot and the lattice parameter. Blue colour (darkest grey in black and white printing) corresponds to the conducting and yellow (lightest grey) to the insulating phase. Green (light grey) indicates the phase where only one spin is conductive. Lower: Spin per dot for $N = 1, 3, 4$ and 5 as a function of lattice parameter.

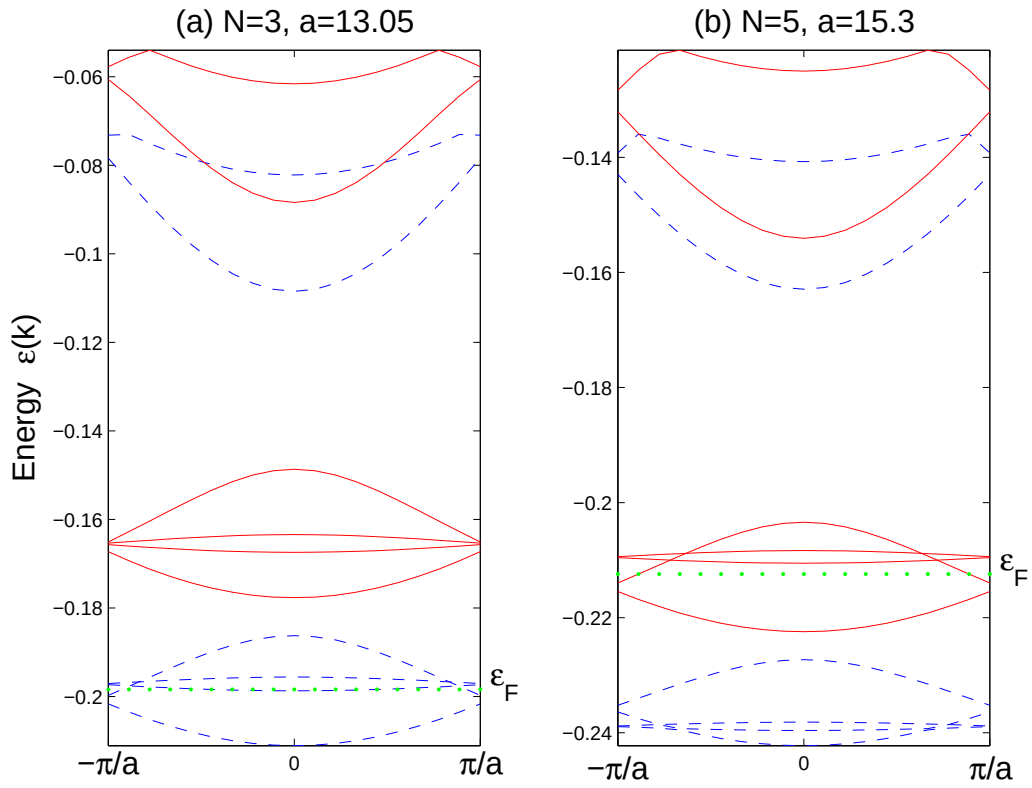

Figure 5.4: p-bands and lowest sd-bands for (a) $N = 3$ at $a = 13.05\ a_0^*$ and (b) $N = 5$ at $a = 15.3\ a_0^*$. The spin-down bands are plotted with blue dashed lines, and the spin-up bands correspond to red solid lines.

the spin degeneracy is restored as kinetic energy contribution becomes dominant. However, a small spin-splitting is regained at $a = 3.14\ a_0^*$ as shown in Figure 5.2.

Figure 5.4 shows that the bands of minority spin are pushed up in energy by exchange splitting and, at an appropriate value of lattice parameter, the Fermi-level resides solely on a single spin band suggesting that only one spin contributes to conductivity. A similar behaviour is observed with $N = 5$. There are now three p-electrons with almost full shell. This spin-dependent conductivity of linear quantum dot chains might be used as a spin filter.

At half-filled p-shell ($N = 4$) Hund's rule leads to maximised spin in an isolated dot. In an array, the spin is at its maximum at $a \approx 18\ a_0^*$ and it decreases gradually with a. The array is an anti-ferromagnetic insulator due to the Fermi-gap induced by the exchange-splitting. For $N = 6$, the p-shell is full and the array remains non-magnetic at all values of a.

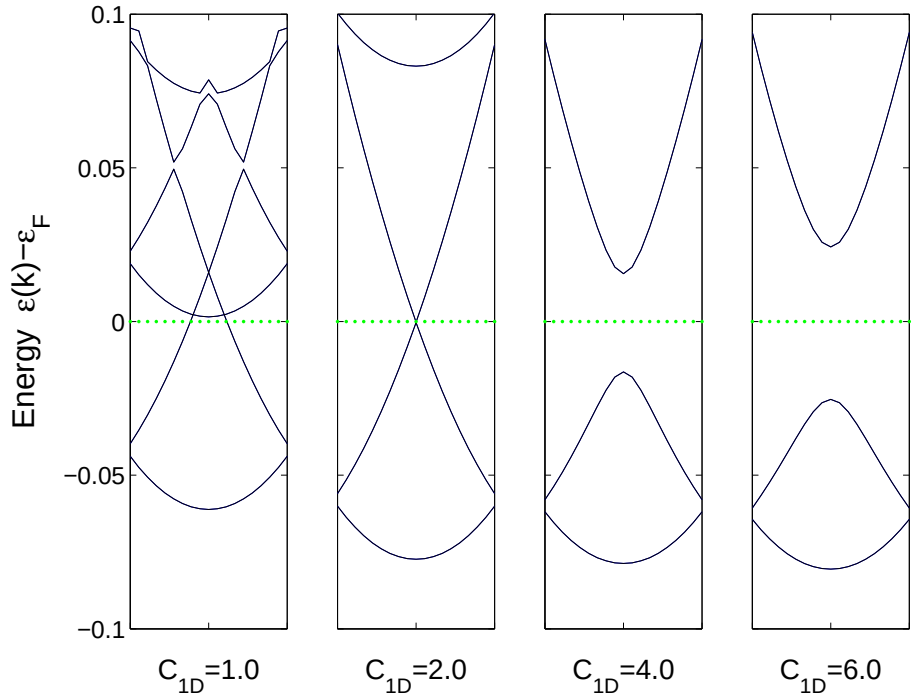

Figure 5.5: Lowest bands at selected values of width parameter C_{1D} for a quantum wire with four electrons per unit cell. The dashed green line indicates the Fermi-level fixed at zero energy.

5.2 Spin-Peierls Transition in Homogenous Quantum Wires

At small values of lattice parameter a, a quantum dot array forms a nearly homogenous quantum wire with a Gaussian cross-section. The background charge distribution for a homogenous wire is chosen to be

$$\rho_B(x,y) = \frac{1}{2r_s^{1D}} \frac{1}{\sqrt{2\pi}\alpha} \exp(-\frac{y^2}{2\alpha^2}), \tag{5.4}$$

where r_s^{1D} is the one-dimensional density parameter. The wire lies along the x-axis, and its width is measured by the full width at half maximum, that is, $2\sqrt{2\ln 2}\alpha$. Since there is no definite lattice parameter for the wire, the length L of the unit cell is chosen in such a way that ρ_B integrates to the desired charge Ne. Thus, we have $L = 2r_s^{1D}N$. We have chosen four electrons to be in the unit cell ($N = 4$) and we have fixed $r_s^{1D} = 2\ a_B^*$. In addition, we define parameter C_{1D} as follows: $C_{1D} = 2r_s^{1D}/\alpha$. It describe the ratio of the average inter-electron separation and the width of the wire: when C_{1D} increases, the wire becomes narrower.

Figure 5.5 shows band structures of a homogenous quantum wire for selected widths.

For $C_{1D} = 2$, the dispersion is parabolic and the Fermi-level lies close to the second transverse sub-band. In this case, the wire shows no magnetism. Antiferromagnetism sets on at $C_{1D} = 4$, as the spin-Peierls transition occurs. The ground state is a spin density wave with wave length of $L/2 = r_s^{1D} N = 8\ a_B^*$. The spin-Peierls transition opens a gap at the Fermi-level and turns the wire into an insulator. The amplitude of the spin density wave increases when C_{1D} increases.

6 Summary and Conclusions

The subject of this thesis was to study the electronic and magnetic properties of coupled quantum dot structures and to develop exchange-correlation energy functional for homogenous fermion gas containing interacting particles with different internal degrees of freedom. The choice for computational method was the Kohn-Sham formulation of the density-functional theory, which is flexible enough for the coupled systems and yet describes correlation effects reasonably well.

In publication [I] we studied the properties of an electron-hole double quantum dot. We constructed a ground state phase diagram as a function of the inter-dot separation and confinement strength. The main aspect of the phase diagram is the competition between Jahn-Teller deformation and Hund's rule as the parameters are varied. Both mechanisms resolve degeneracies when the dots have half-filled shells. In addition, the Coulomb attraction localises electrons and holes into bound dipoles or excitons as the density is lowered.

An extension of the exchange-correlation energy to multicomponent electron gas is introduced in publication [II] and this extension is applied to a quantum dot in publication [III]. Multicomponent electron (or hole) gas could be formed in multilayered heterostructures such as double quantum dots or in systems where the carriers originate from several bands. Examples of such heterostructures are the *multivalley* silicon quantum dots and hole quantum dots where the holes belong to bands with heavy and light effective mass.

The proposed exchange-correlation energy parametrisation agrees well with the existing quantum Monte Carlo data. However, there is a need for more total energy calculations of multicomponent systems in order to construct more accurate interpolation formulas.

For multicomponent quantum dots, the fact that electrons can access more than one internal state eases the localisation at low densities. At higher densities the shell structure is revealed in the addition energy spectrum. The degenerate levels are occupied in accordance to Hund's rule. The degeneracies are lifted as the components have different masses and even a rather small mass difference pushes the levels of heavier mass down in energy leaving lighter components unoccupied.

Publication [IV] presents magnetic and electronic properties of linear one-dimensional

few-electron quantum dot arrays. These properties depend on the inter-dot separation and the number of electrons per unit cell. When the dots are close to each another, the electron densities overlap strongly leading to nearly homogenous quantum wire. The wires are non-magnetic, but they undergo spin-Peierls transition as they are squeezed narrower to become more one-dimensional. At larger dot separations the spin arrangement follows the shell filling of the individual quantum dots. For cases where there is odd number of electrons per quantum dot, the exchange splitting lifts the spin degeneracy, and at certain inter-dot separations the Fermi-level resides solely on a single spin band. This opens an interesting possibility to use a linear dot chain as a spin filter.

References

[I] K. Kärkkäinen, M. Koskinen, M. Manninen, and S.M. Reimann, *Electron-hole bilayer quantum dots: phase diagram and exciton localization*, Solid State Comm. **130** (2004) 187-191

[II] K. Kärkkäinen, M. Koskinen, S.M. Reimann, and M. Manninen, *Exchange-correlation energy of a multicomponent two-dimensional electron gas*, Phys. Rev. B **68**, 205322 (2003)

[III] K. Kärkkäinen, M. Koskinen, S.M. Reimann, and M. Manninen, *Density-functional theory of multicomponent quantum dots*, Phys. Rev. B **70**, 195310 (2004)

[IV] K. Kärkkäinen, M. Koskinen, S.M. Reimann, and M. Manninen, *Magnetism in one-dimensional quantum dot arrays*, cond-mat/0505036

[1] M. P. Marder, *Condensed Matter Physics* (Wiley, New York, 2000)

[2] G. D. Mahan, *Many-Particle Physics* (Plenum Press, New York, 1981)

[3] D. Bimberg, M. Grundmann, and N. N. Ledentsov, *Quantum Dot Heterostructures* (Wiley, England, 1999)

[4] T. Chakraborty *Quantum Dots: A Survey of the Properties of Artificial Atoms* (North-Holland, Amsterdam, 1999)

[5] A. Szabo and N. S. Ostlund, *Modern Quantum Chemistry: Introduction to Advanced Electronic Structure Theory* (McGraw-Hill, New York, 1989)

[6] K. Heyde, *The Nuclear Shell Model* (Springer-Verlag, Berlin, 1990)

[7] H. Haug, S. W. Koch, *Quantum Theory of the Optical and Electronic Properties of Semiconductors* (World Scientific, Singapore, 1990)

[8] R. B. Parr and W. Yang, *Density-Functional Theory of Atoms and Molecules* (Oxford Univ. press, New York, 1989)

[9] J. Stangl, V. Holý, G. Bauer, *Structural properties of self-organized semiconductor nanostructures*, Rev. Mod. Phys. **76**, 725 (2004)

[10] J. M. Elzerman, R. Hanson, J. S. Greidanus, L. H. Willems van Beveren, S. De Franceschi, L. M. K. Vandersypen, S. Tarucha, and L. P. Kouwenhoven, *Few-electron quantum dot circuit with integrated charge read out*, Phys. Rev. B **67**, 161308(R) (2003)

[11] G. Burkard, D. Loss, and D. P. DiVincenzo, *Coupled quantum dots as quantum gates*, cond-mat/9808026 (1998)

[12] T. Ando, A.B. Fowler, and F. Stern, *Electronic properties of two-dimensional systems*, Rev. Mod. Phys. **54**, 437 (1982)

[13] U. Meirav, M. A. Kastner, and S. J. Wind, *Single-electron charging and periodic conductance resonances in GaAs nanostructures*, Phys. Rev. Lett **65**, 771 (1990)

[14] M. A. Reed, J. N. Randall, R.J. Aggarwall, *Observation of discrete electronic states in a zero-dimensional semiconductor nanostructure*, R.J. Matyi, T.M. Moore, and A.E. Wetsel, Phys. Rev. Lett **60**, 535 (1988)

[15] S. Tarucha, D.G. Austing, T. Honda, R.J. vander Hage, and L.P. Kouwenhoven, *Shell Filling and Spin Effects in a Few Electron Quantum Dot*, Phys. Rev. Lett **77**, 3613 (1996)

[16] S.M. Reimann, M. Koskinen, J. Kolehmainen, M. Manninen, D.G. Austing, S. Tarucha, *Electronic and magnetic structure of artificial atoms*, Eur. Phys. J. D **9**, 105 (1999)

[17] P. Hohenberg and W. Kohn, *Inhomogeneous Electron Gas*, Phys. Rev. **136**, B864 (1964)

[18] M. Levy, *Electron densities in search of Hamiltonians*, Phys. Rev. A **26**, 1200 (1982)

[19] E.H. Lieb, *Density functionals for coulomb systems*, Int. J. Quantum Chem. **24**, 243 (1983)

[20] W. Kohn and L. Sham, *Self-Consistent Equations Including Exchange and Correlation Effects*, Phys. Rev. **140**, A1133 (1965)

[21] U. von Barth and L. Hedin, *A local exchange-correlation potential for the spin polarized case*, J. Phys. C. **5**, 1629 (1972)

[22] G. Vignale and M. Rasolt, *Density-functional theory in strong magnetic fields*, Phys. Rev. Lett. **59**, 2360 (1987)

[23] R.O. Jones and O. Gunnarsson, *The density functional formalism, its applications and prospects*, Rev. Mod. Phys. **61**, 689 (1989)

[24] M. Gell-Mann and K.A. Brueckner, *Correlation Energy of an Electron Gas at High Density*, Phys. Rev. **106**, 364 (1957)

[25] J. P. Perdew and Y. Wang, *Accurate and simple analytic representation of the electron-gas correlation energy*, Phys. Rev. B **45**, 13 244 (1992)

[26] T. L. Beck, *Real-space mesh techniques in density-functional theory*, Rev. Mod. Phys. **72**, 1041 (2000)

[27] M. Heiskanen, T. Torsti, M. J. Puska, and R. M. Nieminen, *Multigrid method for electronic structure calculations*, Phys. Rev. B **63**, 245106 (2001)

[28] W. M. C. Foulkes, L. Mitas, R. J. Needs and G. Rajagopal, *Quantum Monte Carlo simulations of solids*, Rev. Mod. Phys. **73**, 33 (2001)

[29] D. M. Ceperley, *Path integrals in the theory of condensed helium*, Rev. Mod. Phys. **67**, 279 (1995)

[30] S.-R. Eric Yang, A. H. MacDonald, and M. D. Johnson, *Addition spectra of quantum dots in strong magnetic fields*, Phys. Rev. Lett. **71**, 3194 (1993)

[31] F. Pederiva, C.J. Umrigar, and E. Lipparini, *Diffusion Monte Carlo study of circular quantum dots*, Phys. Rev. B **62**, 8120 (2000)

[32] F. Pederiva, C.J. Umrigar, and E. Lipparini, *Erratum: Diffusion Monte Carlo study of circular quantum dots [Phys. Rev. B 62, 8120 (2000)]*, Phys. Rev. B **68**, 089901 (2003)

[33] S. M. Reimann, M. Koskinen, and M. Manninen, *Formation of Wigner molecules in small quantum dots*, Phys. Rev. B **62**, 8108 (2000)

[34] R. Egger, W. Häusler, C.H. Mak, and H. Grabert, *Crossover from Fermi Liquid to Wigner Molecule Behavior in Quantum Dots*, Phys. Rev. Lett. **82**, 3320 (1999)

[35] C. Yannouleas and U. Landman, *Collective and Independent-Particle Motion in Two-Electron Artificial Atoms*, Phys. Rev. Lett. **85**, 1726 (2000)

[36] M. Koskinen, M. Manninen, B. Mottelson, and S.M. Reimann, *Rotational and vibrational spectra of quantum rings*, Phys. Rev. B **63**, 205323 (2001)

[37] S. Frauendorf, *Spontaneous symmetry breaking in rotating nuclei*, Rev. Mod. Phys. **73**, 463 (2001)

[38] H. Häkkinen, J. Kolehmainen, M. Koskinen, P.O. Lipas, and M. Manninen, *Universal Shapes of Small Fermion Clusters*, Phys. Rev. Lett. **78**, 1034 (1997)

[39] A. Harju, E. Räsänen, H. Saarikoski, M. J. Puska, and R. M. Nieminen, *Broken symmetry in density-functional theory: Analysis and cure*, Phys. Rev. B **69**, 153101 (2004)

[40] T.H. Oosterkamp, T. Fujisawa, W.G. van der Wiel, K. Ishibashi, R. V. Hijman, S. Tarucha, L.P. Kouwenhoven, *Microwave spectroscopy of a quantum-dot molecule*, Nature **395**, 873 (1998)

[41] W. G. van der Wiel, S. De Franceschi, J. M. Elzerman, T. Fujisawa, S. Tarucha, and L. P. Kouwenhoven, *Electron transport through double quantum dots*, Rev. Mod. Phys. **75**, 1 (2003)

[42] F. Troiani, U. Hohenester, and E. Molinari, *Electron-hole localization in coupled quantum dots*, Phys. Rev. B **65**, 161301-1 (2002)

[43] D.G. Austing, T. Honda, K. Muraki, Y. Tokura, S. Tarucha, *Quantum dot molecules*, Physica B **249-251** (1998) 206-209

[44] B. Partoens and F.M. Peeters, *Molecule-Type Phases and Hund's Rule in Vertically Coupled Quantum Dots*, Phys. Rev. Lett. **84**, 4433 (2000)

[45] H. Imamura, P.A. Maksym, and H. Aoki, *Vertically coupled double quantum dots in magnetic fields*, Phys. Rev. B **59**, 5817 (1998)

[46] U. Sivan, P.M. Solomon, and H. Shrtrikman, *Coupled electron-hole transport*, Phys. Rev. Lett. **68**, 1196 (1992)

[47] T. P. Marlow, L. J. Cooper, D. D. Arnone, N. K. Patel, D. M. Whittaker, E. H. Linfield, D. A. Ritchie, and M. Pepper, *Ground State of a Two-Dimensional Coupled Electron-Hole Gas in InAs/GaSb Narrow Gap Heterostructures*, Phys. Rev. Lett. **82**, 2362 (1999)

[48] T. Kreibich, and E.K.U. Gross, *Multicomponent Density-Functional Theory for Electrons and Nuclei*, Phys. Rev. Lett. **86**, 2984 (2001)

[49] C. Attaccalite, S. Moroni, P. Gori-Giorgi, and G.B. Bachelet, *Correlation Energy and Spin Polarization in the 2D Electron Gas*, Phys. Rev. Lett. **88**, 256601 (2002)

[50] S. Conti and G. Senatore, *Electron correlation and charge transfer instability in bilayered two-dimensional electron gas*, Europhys. Lett. **36**, 695 (1996)

[51] V. Apaja, J. Halinen, V. Halonen, E. Krotscheck, and M. Saarela, *Charged-boson fluid in two and three dimensions*, Phys. Rev. B **55**, 12 925 (1997)

[52] V.M. Bedanov, and F.M. Peeters, *Ordering and phase transitions of charged particles in a classical finite two-dimensional system*, Phys. Rev. B **49**, 2667 (1994)

[53] I. Žutić, J. Fabian and S. Das Sarma, *Spintronics: Fundamentals and applications*, Rev. Mod. Phys. **76**, 323 (2004).

[54] K.J. Thomas, J.T. Nicholls, M.Y. Simmons, M. Pepper, D.R. Mace, and D.A. Ritchie, *Possible Spin Polarization in a One-Dimensional Electron Gas*, Phys. Rev. Lett. **77**, 135 (1996).

[55] K.S. Pyshkin, C.J.B. Ford, R.H. Harrell, M. Pepper, E.H. Linfield, and D.A. Ritchie, *Spin splitting of one-dimensional subbands in high quality quantum wires at zero magnetic field*, Phys. Rev. B **62**, 15 842 (2000).

[56] R.M. Potok, J.A. Folk, C.M. Marcus, and V. Umansky, *Detecting Spin-Polarized Currents in Ballistic Nanostructures*, Phys. Rev. Lett. **89**, 266602 (2002).

[57] J.A. Folk, R.M. Potok, C.M. Marcus, and V. Umansky, *A Gate-Controlled Bidirectional Spin Filter Using Quantum Coherence*, Science **299**, 679 (2003).

[58] L.P. Kouwenhoven, F.W.J. Hekking, B.J. van Wees, C.J.P.M. Harmans, C.E. Timmering, and C.T. Foxon, *Transport through a finite one-dimensional crystal*, Phys. Rev. Lett. **65**, 361 (1990).

[59] H. Tamura, K. Shiraishi, T. Kimura, and H. Takayanagi, *Flat-band ferromagnetism in quantum dot superlattices*, Phys. Rev. B **65**, 085324 (2002).

[60] B. Tanatar and D.M. Ceperley, *Ground state of the two-dimensional electron gas*, Phys. Rev. B **39**, 5005 (1989).

[61] S. M. Reimann and M. Manninen, *Electronic structure of quantum dots*, Rev. Mod. Phys. **74**, 1283 (2002)